# Seismic characterization of timber-masonry connections based on experimental results

Mirra, Michele; Ravenshorst, Geert

**Publication date**
2019

**Document Version**
Final published version

**Citation (APA)**
Mirra, M., & Ravenshorst, G. (2019). *Seismic characterization of timber-masonry connections based on experimental results*. Delft University of Technology.

| | |
|---|---|
| *Project number* | CS2B04 |
| *File reference* | CS2B04WP2-4.3 |
| *Date* | 4th December 2019 |
| *Corresponding author* | Geert J.P. Ravenshorst (g.j.p.ravenshorst@tudelft.nl) |

*TU Delft research program 2018/2019 – WP2*

# SEISMIC CHARACTERISATION OF TIMBER-MASONRY CONNECTIONS BASED ON EXPERIMENTAL RESULTS

*Authors: Michele Mirra, Geert Ravenshorst*

***Cite as**: Mirra, M., Ravenshorst, G. J. P. Seismic characterisation of timber-masonry connections based on experimental results. Report no. CS2B04WP2-4.3, 4th December 2019. Delft University of Technology.*



This research work was funded by NAM Structural Upgrading stream.

# Table of Contents

1 Introduction ..... 4
2 Tested timber-masonry connection configurations ..... 5
2.1 Introduction ..... 5
2.2 Configuration type A (as-built) ..... 6
2.3 Configuration type B (as-built) ..... 7
2.4 Configuration type C (strengthened) ..... 7
2.5 Configuration type D (strengthened) ..... 8
2.6 Configuration type E (strengthened) ..... 8
2.7 Configuration type F (strengthened) ..... 9
2.8 Configuration type G (strengthened) ..... 9
2.9 Sign conventions ..... 10
3 Interpretation of the test results ..... 12
3.1 General ..... 12
3.2 Failure mechanisms ..... 12
3.2.1 Configuration A ..... 12
3.2.2 Configuration B ..... 13
3.2.3 Configuration C ..... 14
3.2.4 Configuration D ..... 17
3.2.5 Configuration E ..... 19
3.2.6 Configuration F ..... 21
3.2.7 Configuration G ..... 23
3.3 Analysis of the response of the connections ..... 26
3.3.1 General ..... 26
3.3.2 Configuration A ..... 27
3.3.3 Configuration B ..... 29
3.3.4 Configuration C ..... 35
3.3.5 Configuration D ..... 39
3.3.6 Configuration E ..... 43
3.3.7 Configuration F ..... 47
3.3.8 Configuration G ..... 51
3.4 Recommendations for calculation of strengthened joints ..... 55
3.4.1 General ..... 55
3.4.2 Configuration A ..... 55
3.4.3 Configuration B ..... 55
3.4.4 Configuration C ..... 55
3.4.5 Configuration D ..... 56

3.4.6 Configuration E ..... 57
3.4.7 Configuration F ..... 58
3.4.8 Configuration G ..... 58
3.5 Damping properties of the connections ..... 59
4 Conclusions ..... 61
5 References ..... 65

# 1 Introduction

This document presents the interpretation of the test results obtained within the whole 2019 experimental campaign on timber-masonry connections, in as-built and strengthened configurations.
The whole set of results was already provided in [1], in which a detailed overview on the tested configurations is given and the response of the connections under monotonic, cyclic and dynamic loading is shown.
In this document, starting from those results, a deeper analysis is conducted, with special regards to the failure mechanisms which could occur in each type of tested connections, and the determination of the main properties of them, such as strength, stiffness and damping.
The conducted experimental campaign refers to common typologies of two as-built timber-masonry connections, identified as type 1 and 1-b in [2], with five proposed retrofitting solutions; all characteristic values derived from the performed tests are reported in [2] as well. In order to provide an overview on the presence of the as-built tested connections and the field of application of the strengthened versions, it is possible to refer to [3], in which the percentage of unreinforced masonry buildings in the Groningen gas field area is quantified as 77% of the building stock. Among these buildings, the tested connections and retrofitting measures pertain to the following building typologies:

- **(Semi-)detached houses with flexible timber diaphragms**: around **17%** of the total amount of unreinforced masonry buildings. In these constructions, realized before 1970, as-built connections consisting of mortar pocket or hook anchors can be found at floor(s) level and roof level.
- **Terraced houses with flexible timber diaphragms**: around **24%** of the total amount of unreinforced masonry buildings. In these constructions, realized before 1970, as-built connections consisting of mortar pocket or hook anchors can be found at floor(s) level and roof level.
- **Terraced houses with rigid diaphragms**: around **23%** of the total amount of unreinforced masonry buildings. In these constructions, realized after 1970, as-built connections consisting of mortar pocket or hook anchors can be found at roof level, where the roof was made with timber elements, while the other floors were made of concrete.

# 2 Tested timber-masonry connection configurations

## 2.1 Introduction

A detailed overview of the tested configurations is reported in [1]; the main features of these connections are also recalled in Table 1 (first testing phase) and Table 2 (second testing phase), while in the following sections the pictures showing the different samples are reported with a short description of them.

Table 1 – Tested timber-masonry connection types in the first phase of the campaign

| Configuration | Description | Test types | Specimen names |
|---|---|---|---|
| A | As-built joist-wall connection. Clay bricks single leaf wall with only beam in mortar. See Introduction for the appearance of this connection in URM houses. | 1 monotonic test | A-M-1 |
| | | 3 quasi-static cyclic tests | A-QS-1, A-QS-2, A-QS-3 |
| | | 3 high-frequency dynamic tests | A-HFD-1, A-HFD-2, A-HFD-3 |
| B | As-built joist-wall connection. Clay bricks single leaf wall with hook anchor. See Introduction for the appearance of this connection in URM houses. | 1 monotonic test | B-M-1 |
| | | 3 quasi-static cyclic tests | B-QS-1, B-QS-2, B-QS-3 |
| | | 3 high-frequency dynamic tests | B-HFD-1, B-HFD-2, B-HFD-3 |
| C | Strengthening option for joist-wall connections in sound masonry. Configuration A retrofitted with an angle bracket screwed to the joist and anchored to the wall. | 1 monotonic test | C-M-1 |
| | | 3 quasi-static cyclic tests | C-QS-1, C-QS-2, C-QS-3 |
| | | 3 high-frequency dynamic tests | C-HFD-1, C-HFD-2, C-HFD-3 |
| D | Strengthening option for joist-wall connections in damaged or low quality masonry. Configuration B retrofitted with a further joist anchored to sound masonry and fixed to the existing joist with steel brackets. The hook anchor is disconnected. | 1 monotonic test | D-M-1 |
| | | 3 quasi-static cyclic tests | D-QS-1, D-QS-2, D-QS-3 |
| | | 3 high-frequency dynamic tests | D-HFD-1, D-HFD-2, D-HFD-3 |

Table 2 – Tested timber-masonry connection types in the second phase of the campaign

| Configuration | Description | Test types | Specimen names |
|---|---|---|---|
| E | Clay bricks single leaf wall. Strengthening with an hook anchor nailed to the joist and glued to the wall after being placed in a previously realised incision on it. | 1 monotonic test | E-M-1 |
| | | 3 quasi-static cyclic tests | E-QS-1, E-QS-2, E-QS-3 |
| | | 3 high-frequency dynamic tests | E-HFD-1, E-HFD-2, E-HFD-3 |
| F | Clay bricks single leaf wall. Strengthening with two inclined screws inserted into the joist after drilling in the masonry proper holes, filled with epoxy. | 1 monotonic test | F-M-1 |
| | | 3 quasi-static cyclic tests | F-QS-1, F-QS-2, F-QS-3 |
| | | 3 high-frequency dynamic tests | F-HFD-1, F-HFD-2, F-HFD-3 |
| G | Clay bricks single leaf wall. Strengthening with timber blocks placed on both sides of the existing joist, screwed to it and anchored to the wall. | 1 monotonic test | G-M-1 |
| | | 3 quasi-static cyclic tests | G-QS-1, G-QS-2, G-QS-3 |
| | | 3 high-frequency dynamic tests | G-HFD-1, G-HFD-2, G-HFD-3 |

## 2.2 Configuration type A (as-built)

This first configuration consisted of a simple masonry pocket, therefore the resistance to horizontal loads was given only by friction between timber and mortar. The sample that was built representing this situation is depicted in Figure 1.

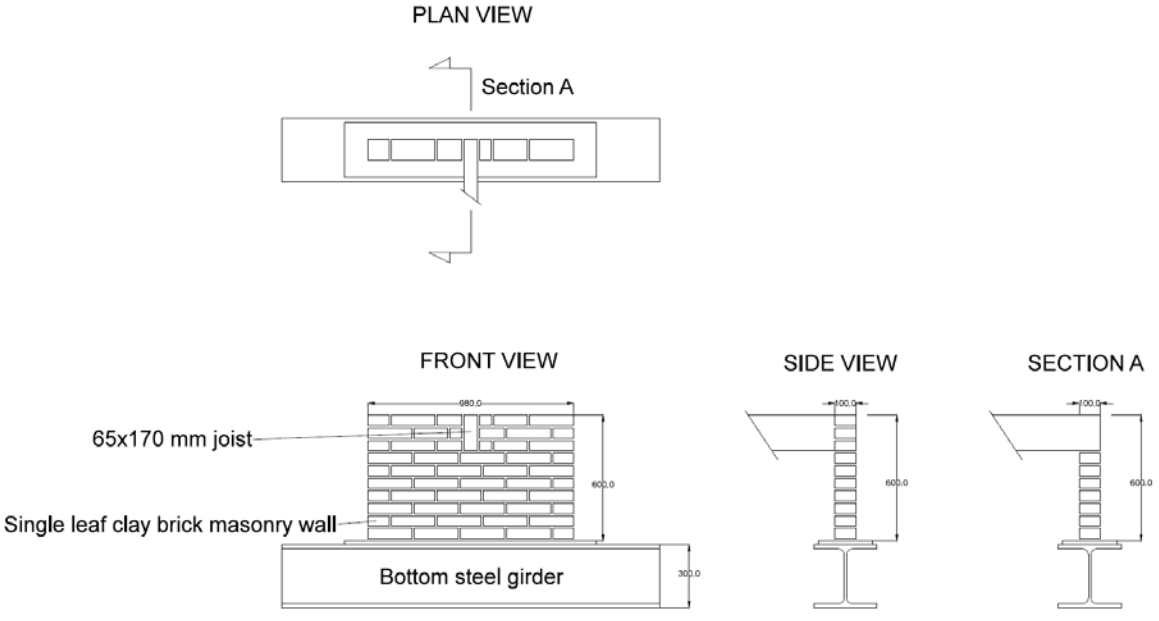


Figure 1 – Sample representing an as-built connection with simple masonry pocket.

## 2.3 Configuration type B (as-built)

This second as-built configuration consisted of an hook anchor connecting the joist to the external side of the wall. The anchor was fastened to the joist by means of 4x55 mm nails and measured 240x240 mm with a diameter of 14 mm. The sample representing this situation is depicted in Figure 2.

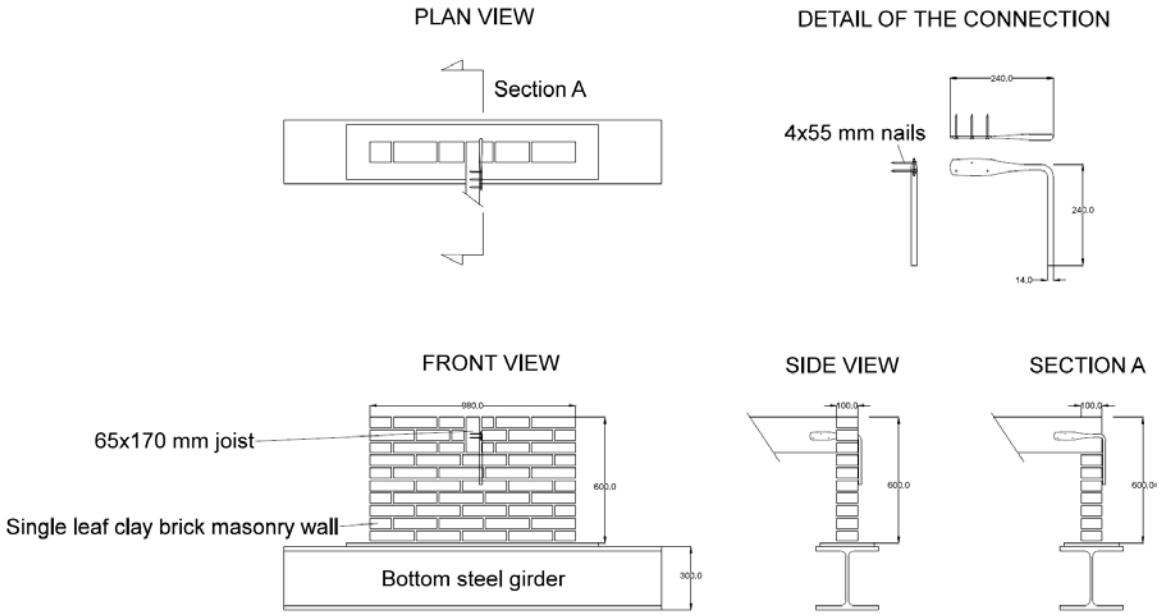


Figure 2 – Sample representing an as-built connection with hook anchor.

## 2.4 Configuration type C (strengthened)

This strengthening option was already tested during the previous pilot study and consisted of a Rothoblaas steel angle (thickness 3 mm, with 2 stiffeners to extend bending moment capacity) anchored to the masonry (10x95 mm anchors) and screwed to the joist (5x60 mm screws). The specimen representing this retrofitted joint is shown in Figure 3.

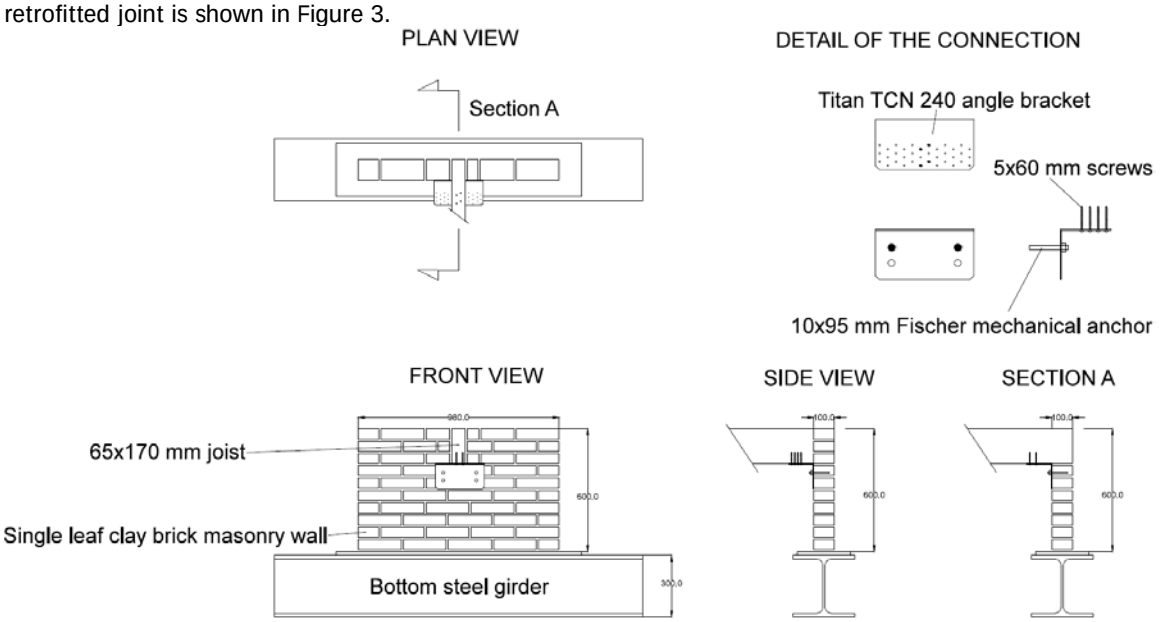


Figure 3 – Sample representing a strengthening option consisting of a steel angle screwed to the joist and anchored to the masonry. This retrofitting technique can be applied when the wall is not damaged.

## 2.5 Configuration type D (strengthened)

This strengthening option was intended to be used in presence of masonry which is damaged around the connection or for low quality masonry at the top rows of the wall. 10x165 mm anchors were used to fasten an additional 65x70 mm joist to sound masonry and two steel brackets with 5x60 mm screws connected this joist to the existing one. The specimen representing the retrofitted connection is shown in Figure 4.
For this last configuration, as can be seen from the figure, the hook anchor was also present because the damaged samples of configuration B were used to test this strengthening option, but it was disconnected from the timber joist before retrofitting these samples.

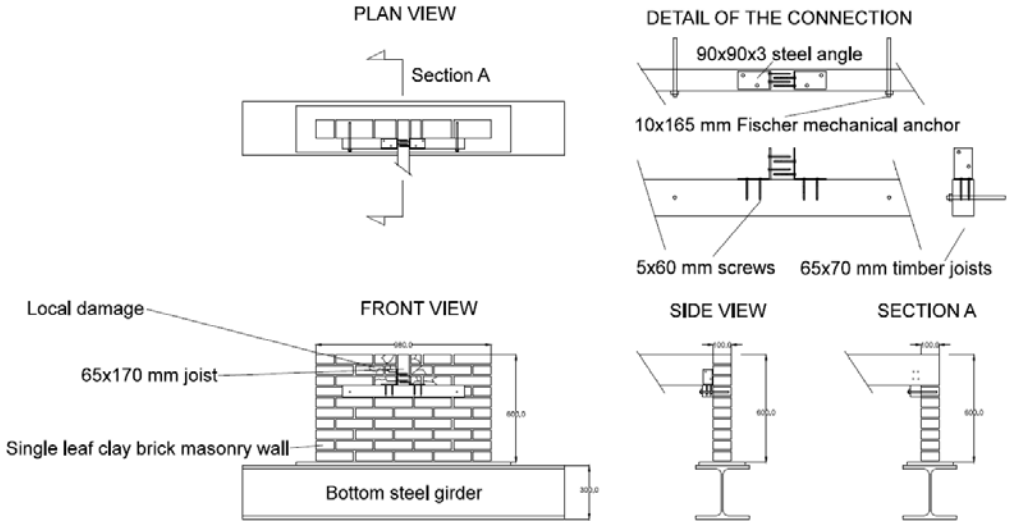


Figure 4 – Sample representing a strengthening option to be applied when the masonry is damaged around the joist. A further joist is anchored to sound masonry and then to the existing joist.

## 2.6 Configuration type E (strengthened)

This strengthening option consisted of a standard 240x240x14 mm hook anchor fastened to the joists by means of 4x55 mm nails and glued to the wall. The anchor was therefore embedded in the glue, which filled a 25x40 mm incision realized on the masonry. Beside the strengthening system, also the influence of the floor planks during the seismic motion was studied. This configuration is shown in Figure 6.

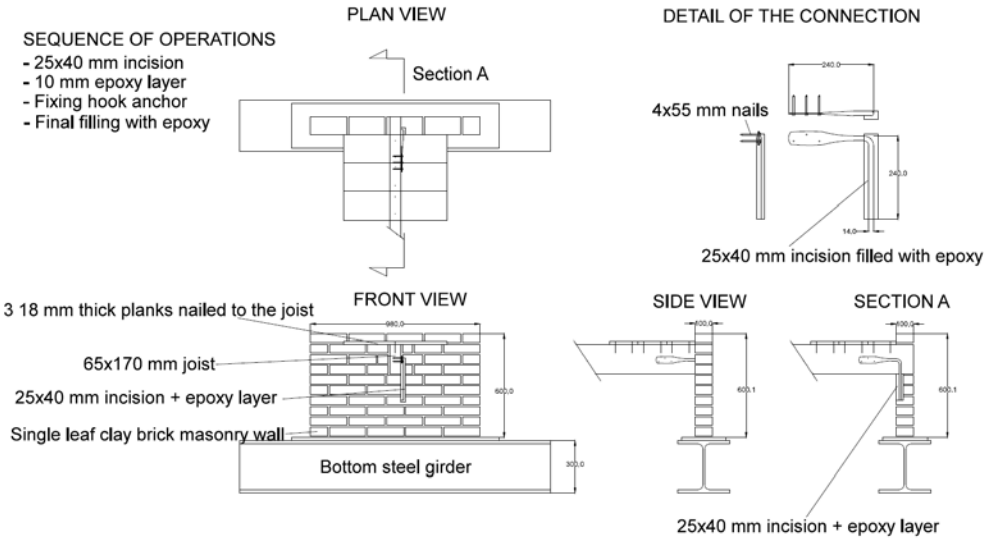


Figure 6 – Sample representing a strengthening option consisting of a hook anchor nailed to the joists and glued to the wall.

## 2.7 Configuration type F (strengthened)

In this configuration 7x180 mm screws were used to connect the joist and the wall. The screws were placed at an angle of 45 degrees both in the vertical and horizontal plane, in order to reach a sounder part of the masonry. Before inserting the screws in the timber joist, 10 mm holes were drilled in the wall and then filled with injected epoxy. This intervention presents an important advantage, because it can be performed from outside. This configuration is shown in Figure 7.

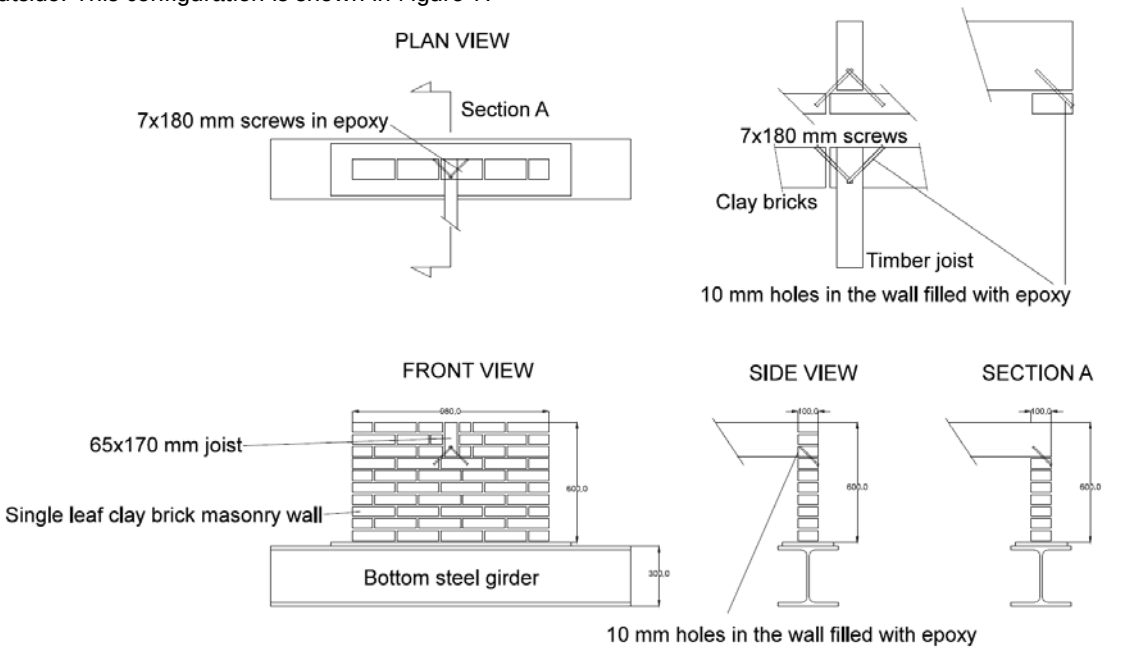


Figure 7 – Sample representing a strengthening option consisting of screws fixed to the timber joist and embedded in epoxy for the whole length of the predrilled hole in the masonry.

## 2.8 Configuration type G (strengthened)

This strengthening option was realized with 65x170 mm timber blocks placed on both sides of the joist (in practice they would be placed between each couple of joists). The blocks were firstly fixed to the existing joist by means of 5x70 mm screws drilled at an angle of 45 degrees, and then fastened to the masonry with 10x165 mm mechanical anchors. However, since this intervention involves in practice also the diaphragm, it was important to recreate the same conditions: hence, beside the presence of the planks, fixed to the joist with 3x65 mm nails, also an additional plywood panel overlay was placed on them and screwed through the planks inside the blocks, as it would happen in practice. This ensured that all the elements of the connections, which were involved in the transfer of the horizontal load, were present.
This configuration is depicted in Figure 8.

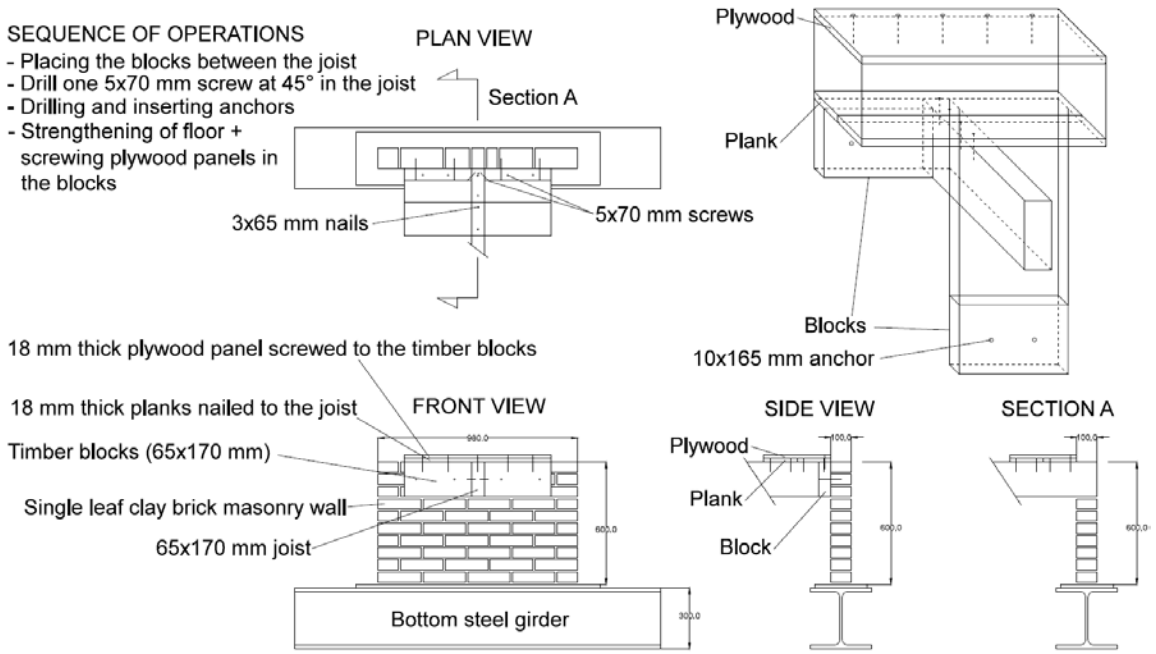


Figure 8 – Sample representing a strengthening option consisting of timber blocks anchored to the masonry and screwed to the joist and to the plywood panel overlay used for the diaphragms' strengthening.

## 2.9 Sign conventions

Figures 9a and 9b show the sign convention used throughout the document and the two most signifying parameters that were recorded: the relative displacement between joist and wall (measured by sensor 3) and the maximum out-of-plane displacement of the wall (measured by sensor 4), as also reported in [1].

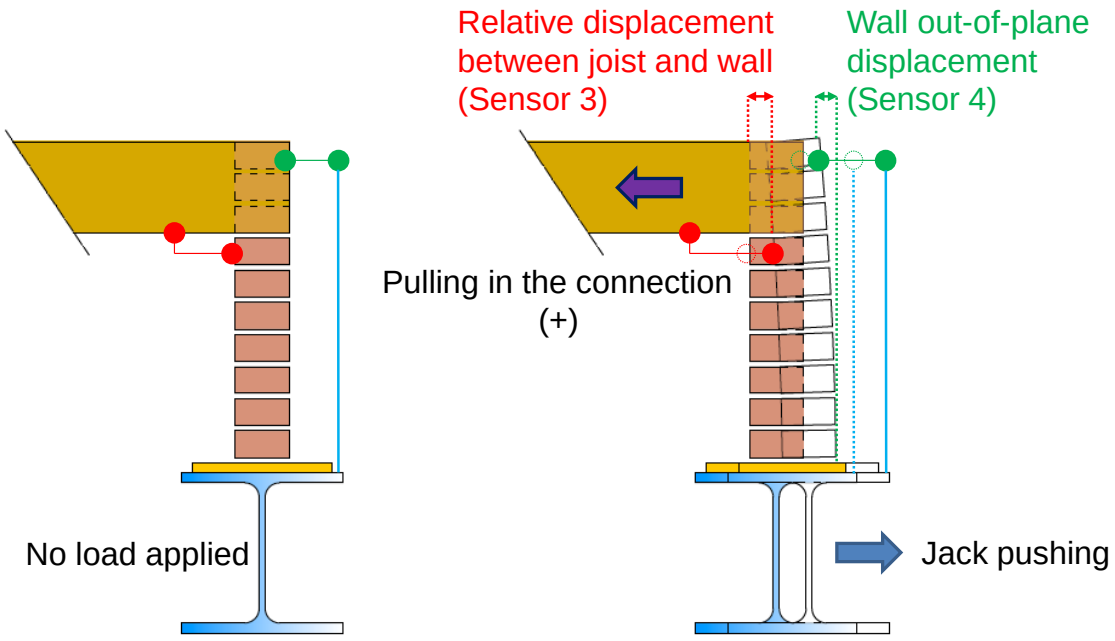


(a)

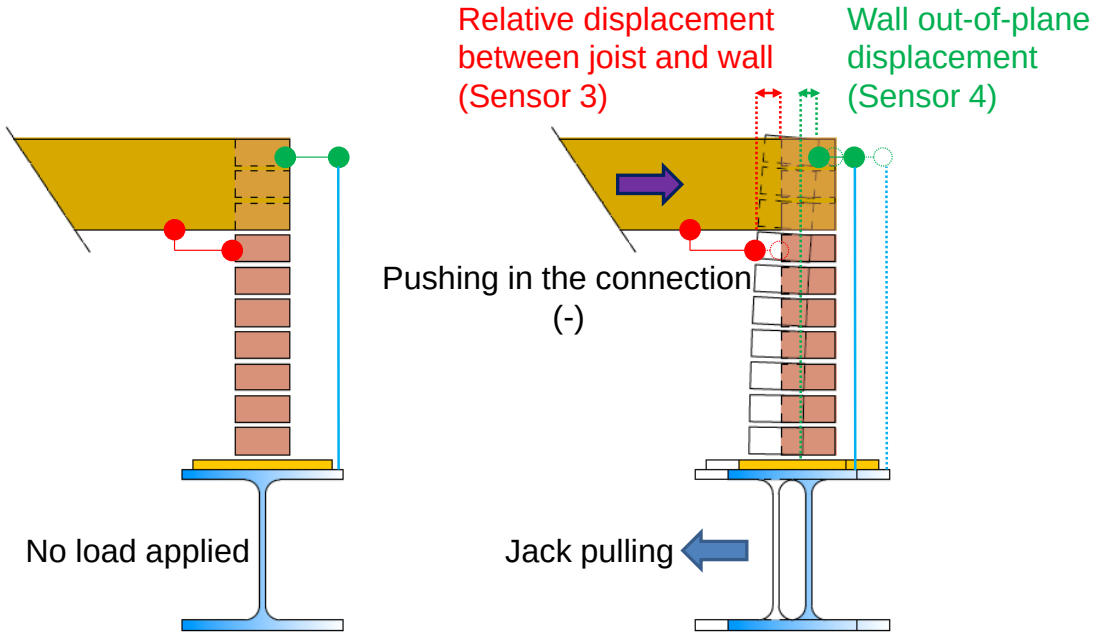


(b)

Figure 9 – Sign convention and signifying parameters when pulling (a) and pushing (b) the connection: both initial and deformed state are shown.

# 3 Interpretation of the test results

## 3.1 General

In this section the analysis of the test results of the seven configurations of timber-masonry connections is conducted. Firstly, for each configuration the failure mechanisms will be analysed; then, the main properties of the connections (strength, stiffness and damping) will be derived, together with the determination of simplified constitutive laws for them.

## 3.2 Failure mechanisms

### 3.2.1 Configuration A

For configuration A (as-built) no real failure of the samples was observed, because of the frictional behaviour of this connection type (Figure 10), with no damage to the walls.
As observed, a slightly tilted joist may increase the final resistance of the connections [1], but by adopting a purely frictional behaviour a safe estimation of the strength of this connection type can be determined, as shown in section 3.3.1. In any case, this increase in strength is given by the fact that a tilted joist can involve friction not only in the bottom part of the masonry pocket, but also on both of its sides.
It is furthermore worth noticing that although the samples were not damaged after testing, in practice this would mean a high risk of out-of-plane collapse of the wall, which are not really connected to the floor joists. This is because as soon as the horizontal load overcomes the frictional force which activates the sliding of the joist in the mortar pocket, a large relative movement between the floor beams and the walls could start. And this sliding takes place with a very low resisting frictional force, not able to prevent the wall from out-of-plane cracking or, in presence of intense earthquakes, from overturning.


Figure 10 – Frictional behaviour of configuration A

### 3.2.2 Configuration B

Configuration B (as-built) was characterized by a strongly non-symmetric behaviour, due to the specific shape of the hook anchor: when the joist was pushed towards the wall, a response similar to configuration A was obtained (mainly frictional behaviour, but with higher values of force); in the opposite direction, instead, the stiffness of the wall was brought into play with higher values of recorded force.
The possible failure mechanisms of this type of connections are therefore:

- When pushing the joist: cracking of mortar and frictional sliding of the hook anchor and the joist (Figure 11);
- When pulling the joist: cracking of masonry (Figure 12) and, should the nails connecting hook anchor and joist not have a large diameter, possible yielding of them or splitting of the joist. This last type of failure was not present in the tested samples because the nails were thick, as also can be found in practice. Thus, the cracking of masonry has to be considered for this loading direction as first and less resisting mechanism.

The failure of the steel hook anchor itself could also be included, but it is very unlikely given its large diameter. From the observations of the tested samples, it can be regarded as a rigid body which can only move and rotate as a whole.

Figure 11 – Cracking of mortar and frictional sliding of the hook anchor

Figure 12 – Cracking of masonry around the hook anchor

### 3.2.3 Configuration C

Configuration C (strengthened) exhibited a large improvement in strength and stiffness of the connection on both loading directions, when compared to the results of A and B samples. Given the different components of this connections, several failure mechanisms can be identified:

1. Pull-out failure of the mechanical anchors connecting the steel angle to the wall (Figure 13a);
2. Extraction from the wall of the bricks in which the mechanical anchors are fastened; this is linked to a shear failure of the bond (Figure 13b);
3. Cracking of masonry around the connection (Figure 14);
4. Bending and yielding of the steel angle (Figure 15);
5. Shear yielding and failure of the screws connecting the steel angle to the joist;

It is important to notice that failure mechanisms 5 was not observed during the tests, but depending on the number and diameter of the screws and on the state of the timber close to the connection, it might also occur in practice, because a slight movement of the screws was detected also during the tests. Moreover, failure mode 5 is desirable because it is the only ductile one, which should therefore govern the global strength, and also the global failure after larger displacements.

(a)

(b)

Figure 13 – Pull-out failure of the mechanical anchors (a) and extraction from the wall of the bricks where the mechanical anchors are fastened (b)

Figure 14 – Cracking of masonry around the connection

Figure 15 – Bending and yielding of the steel angle

### 3.2.4 Configuration D

Configuration D (strengthened) exhibited a large improvement in strength and stiffness of the connection as well, when compared to the results of A and B samples. Given the different components of this connections, several failure mechanisms can be identified:

1. Pull-out failure of the mechanical anchors connecting the additional joist to the wall (Figure 16);
2. Cracking of masonry around the connection (Figure 17);
3. Bending and yielding of the steel brackets (Figure 18) ;
4. Shear yielding and failure of the screws connecting the steel brackets to both joists (Figure 19);
5. Pull-out failure of the screws connecting the steel brackets to the additional joist;
6. Extraction from the wall of the bricks in which the mechanical anchors are fastened; this is linked to a shear failure of the bond;
7. Failure of steel brackets (tear out of one side)

It is important to notice that failure mechanisms 5 to 7 were not observed during the test, but they might also occur in practice and are therefore included in this list. Failure mechanism 5 is linked to the number and diameter of the screws and on the material properties of the additional joist. Failure mechanisms 6 is the same as described for configuration C. Failure mechanism 7 might occur with large diameter fasteners, inducing the shear failure on the brackets after their yielding.
Ductile, and thus desired, failure mechanisms are number 3 and 4.

Figure 16 - Pull-out failure of the mechanical anchors connecting the additional joist to the wall

Figure 17 – Cracking of masonry around the connection

Figure 18 – Bending and yielding of the steel brackets


Figure 19 – Shear yielding of the screws connecting the steel brackets to both joist

### 3.2.5 Configuration E

Configuration E (strengthened) exhibited a stiff response with low energy dissipation. Although this connection is not characterized by many elements, still several failure mechanisms can be identified:

1. Failure of the masonry around which the hook anchor is glued (mainly when loading in tension, Figure 20);
2. Cracking of masonry around the connection (mainly when loading in compression, Figure 21);
3. Bending and yielding of the nails;
4. Detachment of the glued interface;
5. Crack opening or damage within the epoxy layer;
6. Failure of the hook anchor due to excessive rotation or bending;

It is important to notice that failure mechanisms 3 to 6 were not observed during the test, but they might also occur in practice and are therefore included in this list. Compared to test results, failure mechanism 3 should be improved, because no yielding in the nails was detected and that could improve the dissipative properties of this joint type. At the same time, it should be noticed that the fasteners which are normally adopted to connect hook anchors to timber are often characterized by a large diameter (5 mm nails in our case), so high strength of masonry and glued layer is required to bring them into play before other more brittle mechanisms take place. Failure mechanisms 4 did not occur, and this proved the effectiveness of the epoxy layer, because it was able to involve the masonry around it as well. With very poor quality masonry, however, this failure mode should carefully be taken into account because might correspond to an overall lower strength. Failure mechanism 5 is related to the quality of the layer itself: if this is damaged, then the anchor is not contrasted anymore and effective transfer of horizontal force does not occur. Finally, failure mode 6 is mentioned, but it is the most unlikely to happen, due to the large cross section of the hook anchor. With very resistant masonry and high-strength nails it is nevertheless recommended to take it into account.
Only failure modes 3 is are ductile and has to be privileged, with the former that has to be preferred.

Figure 20 – Failure of masonry around the epoxy layer before and after removal of the hook anchor

Figure 21 – Cracking of masonry due to the pushing load of the hook anchor

### 3.2.6 Configuration F

Configuration F (strengthened) exhibited a very stiff response and energy dissipation mainly related to masonry damaging and cracking. The following failure mechanisms can be identified:

1. Failure of the masonry around the holes containing the screws and filled with epoxy (Figure 22);
2. Cracking of masonry around the connection (Figure 23);
3. Bending and yielding of the screws;
4. Pull-out or tensile failure of the screws;

It should be noticed that failure mechanism 3 and 4 were not detected for the tested samples. Failure mode 3 might occur in presence of high strength masonry and very slender fasteners, leading to yielding or bending of screws even before cracks start to occur. Failure mode 4 is also linked to the aforementioned situation, and especially for pull-out failure of the screws from the timber joist, which could occur when the wall is able to withstand high forces.
A desirable and ductile failure mode is number 3; however, in this specific case it is slightly more difficult to achieve this failure mechanism, because the screws are loaded with a combination of shear and axial force, making the whole system less ductile. Penetration length and diameter can still play an important role, as will be highlighted in section 3.4.7.

Figure 22 – Failure of the masonry around the holes containing the screws and filled with epoxy

Figure 23 – Cracking of masonry around the connection

### 3.2.7 Configuration G

Configuration G (strengthened) exhibited a very ductile response with high energy dissipation mainly related to firstly yielding of nails and screws, and then to masonry damaging and cracking. The following failure mechanisms can be identified:

1. Yielding and bending of the nails connecting joist and planks (Figure 24);
2. Yielding and bending of screws connecting the plywood panel to the planks and the timber blocks (Figure 25);
3. Cracking of masonry around the whole connection (Figure 26);
4. Pull-out failure of the mechanical anchors (Figure 27);
5. Bricks extraction around the anchor's position (Figure 28);
6. Yielding, pull-out or tensile failure of the screws connecting the timber blocks to the joist;

It should be noticed that failure mechanism 6 was not detected for the tested samples. It might occur in presence of high strength masonry and very slender fasteners, but it is more unlikely compared to modes 1 and 2 because the transfer of loads occurs from the plywood to the planks, and then from them to the blocks and the wall: therefore, it is more related to the top part of the joint.
Ductile and desired failure modes are number 1, 2 and 6. This variety of possible mechanisms is a good characteristic of this configuration, because it enables quite high energy dissipation.

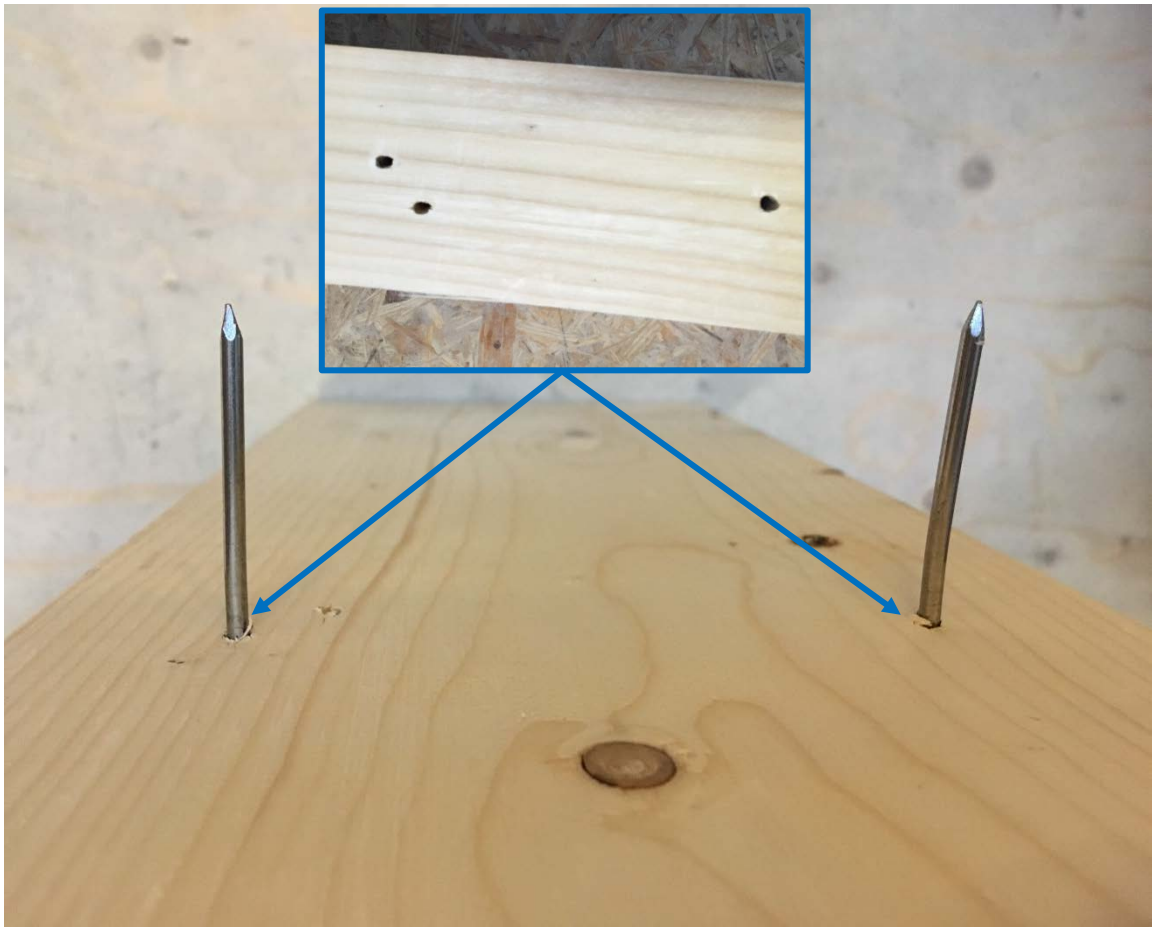

Figure 24 – Bending and yielding of nails connecting the plank to the joist; wood embedment is also shown

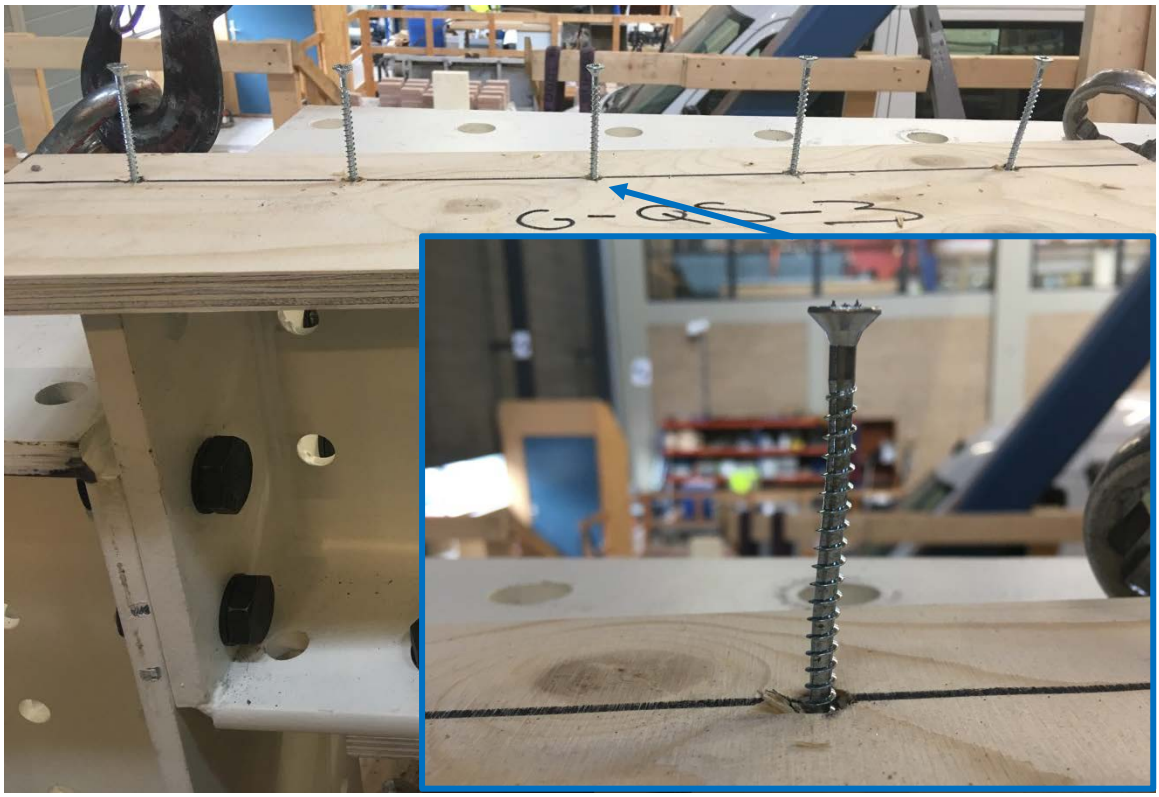

Figure 25 – Bending and yielding of the screws connecting the plywood panels to the planks and the blocks

Figure 26 – Cracking of masonry around the joint

Figure 27 – Pull-out failure of mechanical anchors

Figure 28 – Brick extraction around the anchor's position

## 3.3 Analysis of the response of the connections

### 3.3.1 General

This section presents the analysis and the formulation of constitutive laws for the tested joint configurations. With the exception of configuration A, for all the other connections the constitutive laws will be obtained by adopting a bilinear curve (always reported in red) derived from experimental data points (always reported in blue), for both quasi-static and dynamic tests. These data points correspond to the peak force reached in the first run of each cycle for quasi-static tests (backbone curve), or to the maximum load reached for each signal amplitude in the dynamic tests. This is shown in the example of Figure 29: starting from the backbone curves obtained from the hysteretic cycles, their data points are extracted and reported for the three (quasi-statically or dynamically) tested samples. Based on these data points, a bilinear curve is calculated following the principle of energy equivalence, as is done for instance in pushover analyses.

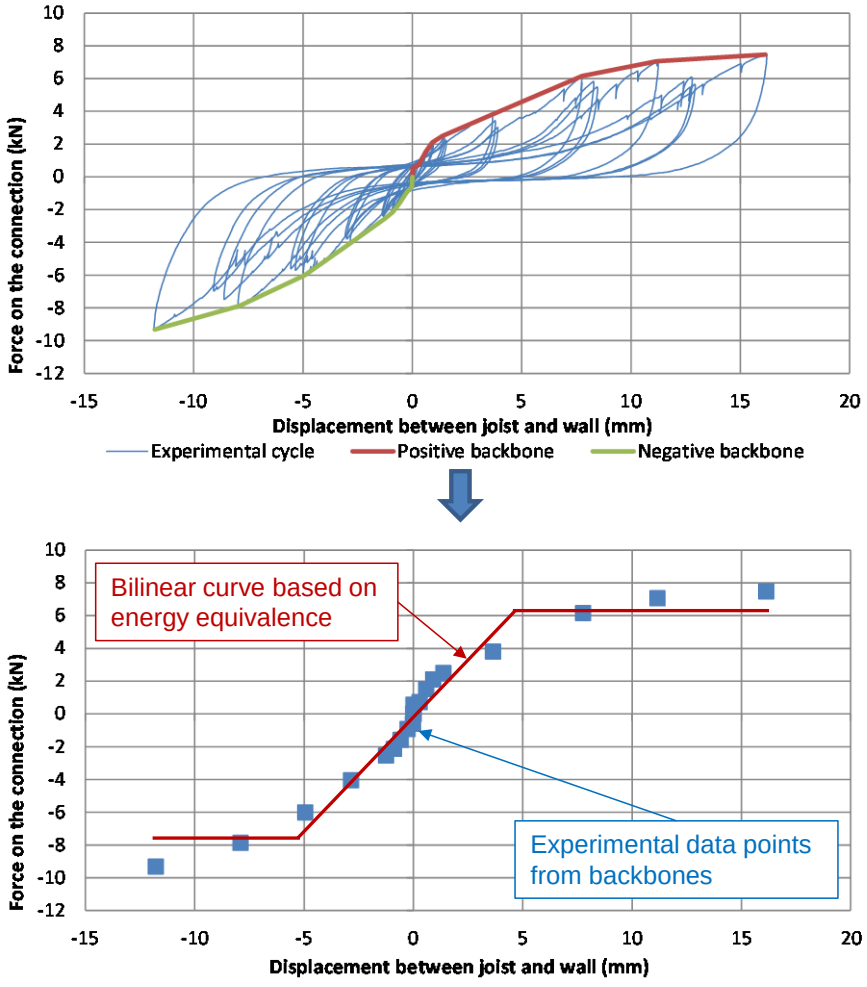


Figure 29 – Example of derivation of bilinear curves for constitutive laws of connections. The reported graphs refer to sample G-QS-1, but the same procedure was followed for the analysis of all configurations.

### 3.3.2 Configuration A

As already stated, this configuration was mainly characterized by a frictional behaviour. Therefore, the resistance of the connection to the horizontal loads can be estimated by applying the usual equations for friction:

- $F_{peak} = \mu_p F_v$ for peak friction (before sliding of the connection)
- $F_{post-peak} = \mu_{pp} F_v$ for post-peak friction (sliding of the connection)

In the reported equations $F_{peak}$ is the horizontal peak force on the connection, $F_{post-peak}$ is the horizontal post-peak force on it, $F_v$ is the vertical force on it, $\mu_p$ and $\mu_{pp}$ are the peak and post-peak friction coefficients, respectively.
The friction model was derived from the characteristic values of force and friction coefficient reported in the Database of connections [2], from which it can be calculated:

- $\mu_p = 0.8$
- $\mu_{pp} = 0.6$

From these values it is possible to obtain a safe estimation of the strength of this connection, as shown in Figure 30a, in which the frictional model with the proposed coefficient is compared to the three performed quasi-static tests and to the monotonic test (which is quite well matched). The comparison with dynamic test results is instead shown in Figure 30b only for sample A-HFD-2 for a better understanding. This is the sample showing the lowest value of strength.
As can be observed, the samples which were actually relying only on friction as resisting mechanism prove to be well predicted by the model. Other effects, such as tilted joists or suddenly applied loads (as it could happen in practice) could increase the resistance, as already stated. The reason for that is the involvement of a larger portion of the masonry pocket, so not only the bottom part but also the sides of it.
This was confirmed by the displacement recorded by sensor 4 [1], placed close to the masonry pocket's side: as shown in Figure 31, when the behaviour is purely frictional, a negligible displacement of the wall is recorded, while with a tilted joist or with a suddenly applied load a larger displacement occurred, which led to higher value of recorded force as well.
As a last aspect, an essential parameter for seismic design is ductility, which ensures that the connection is able to deform until large displacements, providing beneficial energy dissipation. In this case, it can be easily stated that the mortar pocket is a very ductile joint, but of course the very low strength make this connection not suitable for seismic areas with high demands, because it relies only on friction.

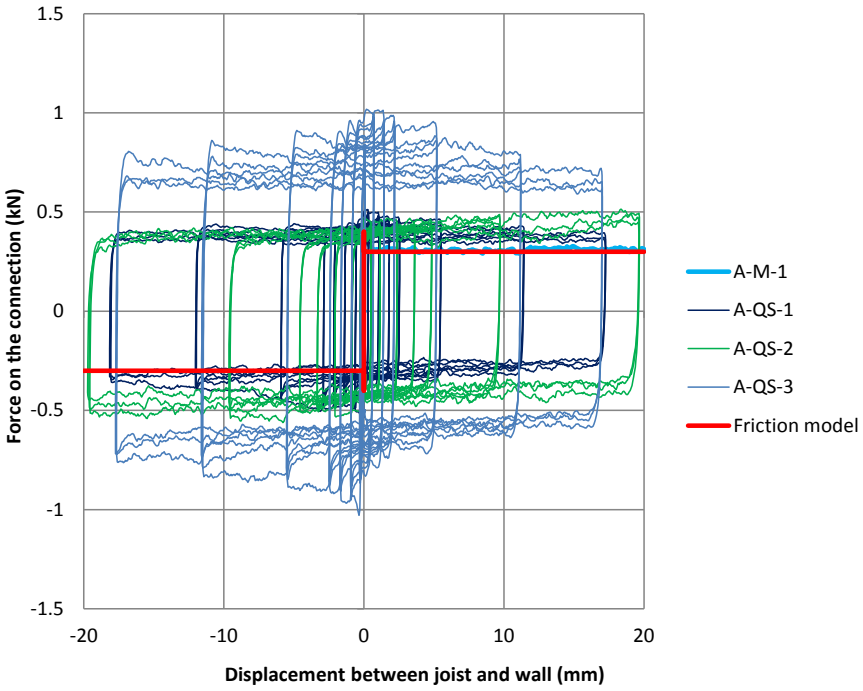


(a)

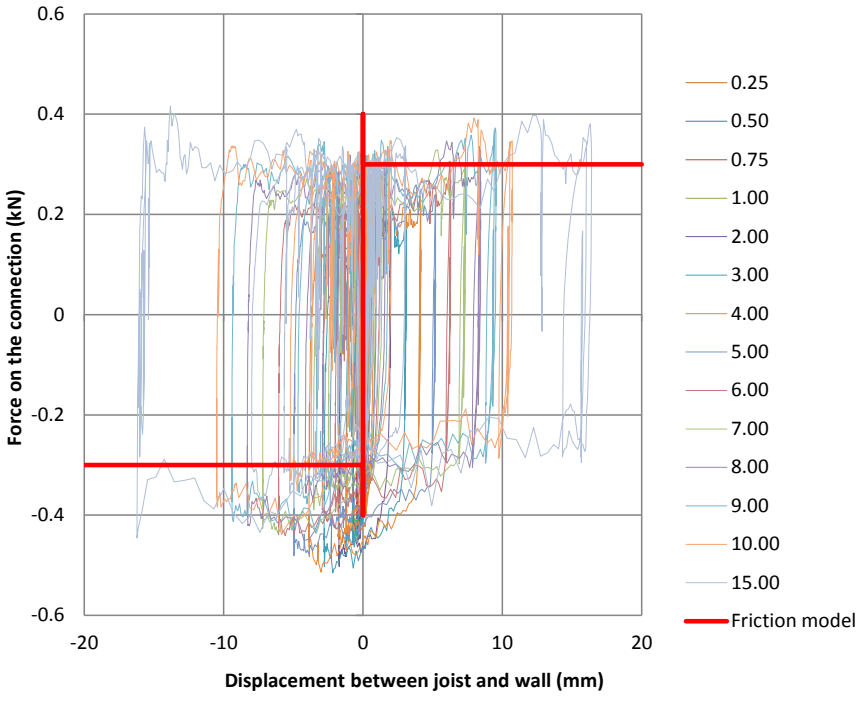


(b)

Figure 30 – (a) Comparison of the performed monotonic and quasi-static tests with the frictional model; (b) comparison between the frictional model and the dynamic response of sample A-HFD-2, showing the lowest strength values.

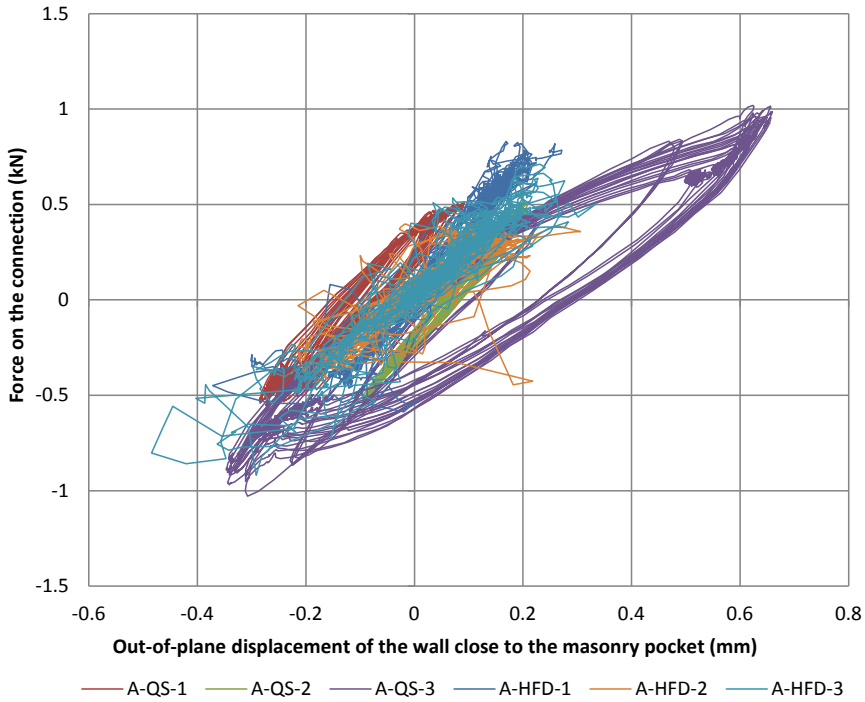


Figure 31 – Comparison of the out-of-plane displacement of the walls among the tested samples. The three samples showing a purely frictional behaviour (A-QS-1, A-QS-2 and A-HFD-2) exhibit a very limited displacement of the wall, while the others displayed a larger displacement correspondent to higher values of recorded force as well.

### 3.3.3 Configuration B

The connection with hook anchor showed a frictional behaviour in pushing, while when pulling it was able to involve a larger portion of masonry with higher values of strength as well [1].
The pushing direction can be considered similar to configuration A with regard to the frictional response. However, in this case, the reached peak forces were higher due to the presence of the sliding hook anchor beside the joist. The further adherence between the anchor and the mortar could involve a larger portion of the wall in the response when pushing: the recorded out-of-plane displacements were between 0.4 to 0.5 mm, and were therefore comparable to the values already shown in Figure 18 for configuration A, when further contributions to friction, beside the one at the bottom of the joists, were present. Results also showed (samples B-QS-3 and B-HFD-3, see [1]) that the presence of mortar particles after cracking in the masonry pocket could cause larger values of strength when pulling, because wall and joist were able to move almost simultaneously.
As for the pulling direction, the involvement of a large part of the wall around the joint could increase the strength of the connection, with however a difference between quasi-static tests and dynamic ones: in the latter cases the maximum recorded forces were lower. This was probably caused by the higher play which occurred to the hook anchor due to the sudden dynamic loading. This fact determined a decrease in stiffness and therefore the process of reaching the peak was much slower than that of quasi-static tests. In fact, in the dynamic tests the actual value of strength was not reached, but only the force corresponding to the largest displacement applied to the connection (15 mm). This is also shown by the amount of damage in the wall: quasi-static tests exhibit in general larger displacement and more cracks than the dynamic tests (Figure 32).
The damage of the wall was also responsible for the shape of the cycles corresponding to large displacements: since the sensor was measuring the relative displacement between joist and wall, when the latter was damaged, it accumulated displacement and therefore influenced the response. This is better clarified in Figure 33, showing the ideal response without accumulated displacement (similar to a monotonic test) and the comparison with the actual cycle for sample B-QS-1.

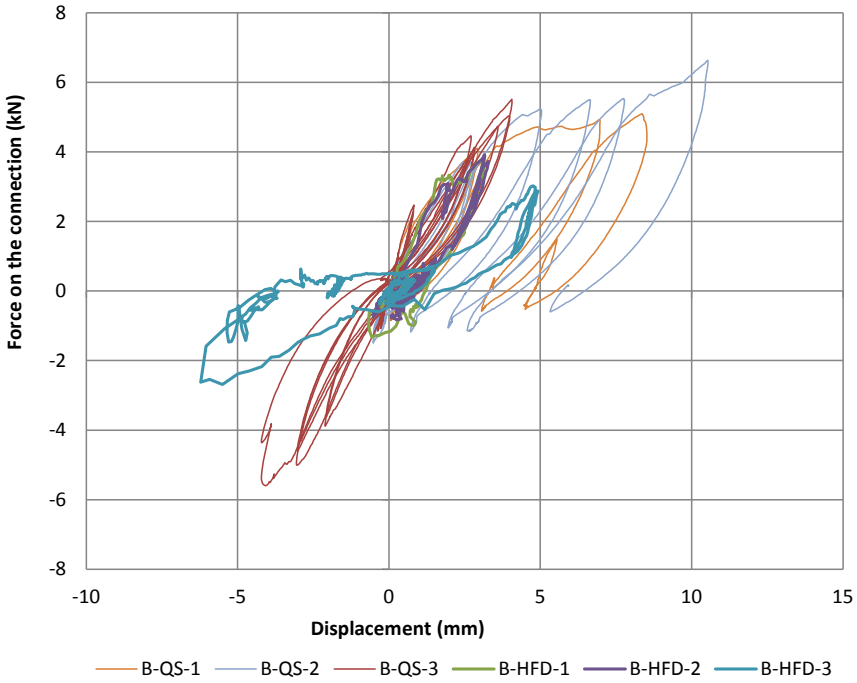


Figure 32 – Comparison among the wall's out-of-plane displacements for quasi-static and dynamic tests: in the former cases the damage and cracking was higher due to the larger displacements accumulated by the wall.

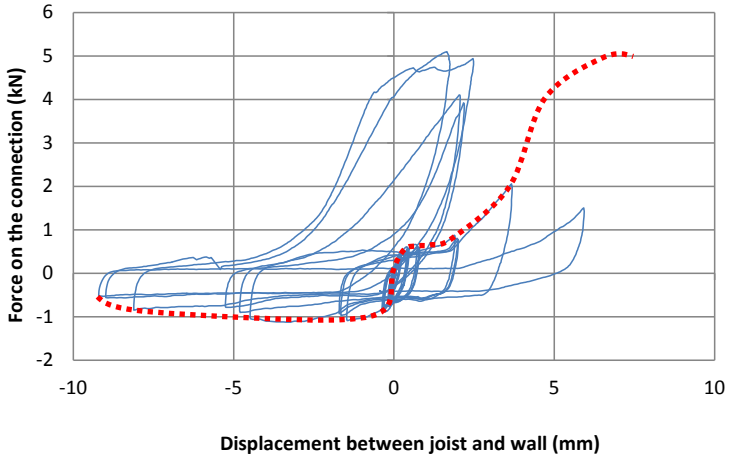


Figure 33 – Comparison between the actual hysteretic cycle of the wall (blue) and the behaviour which would occur without any damage in the wall (red dashed backbone).

This type of connection showed high values of strength for the pulling direction compared to configuration A. It should be noticed, however, that this peak force corresponds to large relative displacements between wall and joist: this fact should be taken into account when studying the out-of-plane response of a wall connected to the floor by means of hook anchors.
After testing, it is also necessary to define constitutive laws for the connection, as it was done for configuration A with frictional model. In this case, the response of the connection can be modelled according to Figure 34.

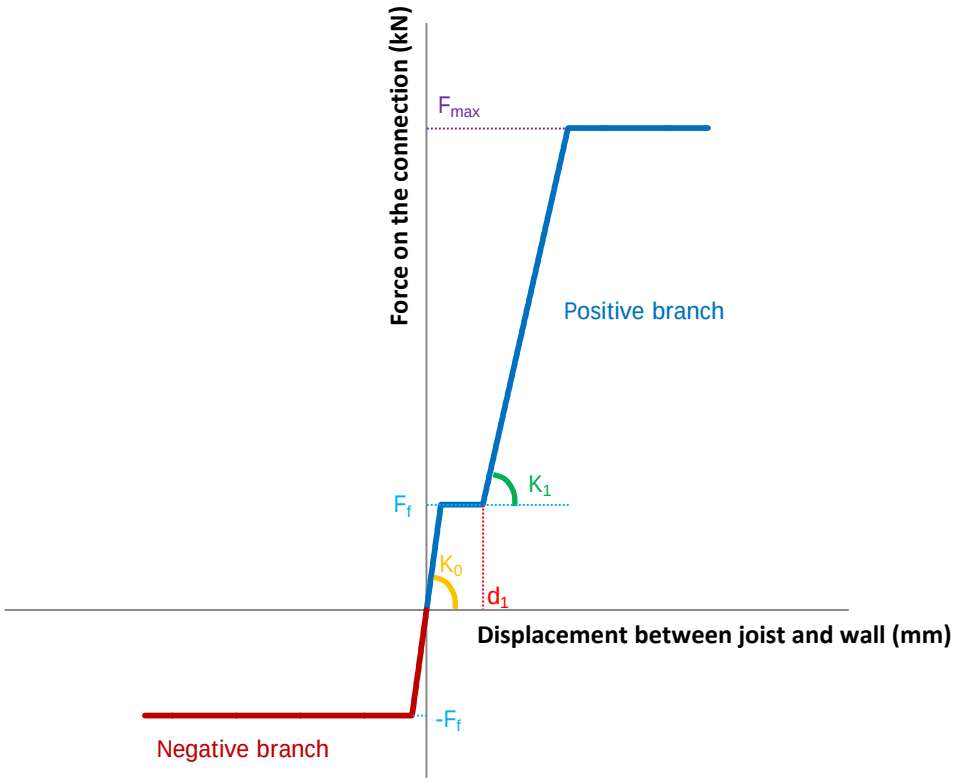


Figure 34 – Simplified model representing the response of the hook anchor connection.

Basically, the frictional model is adapted to the new response of the connection: for the negative branch (pushing), this is still present with a bilinear response having maximum value $F_f$, while for the positive this is extended compared to the previous case: in the initial phases, when the anchor is still not involving the whole portion of wall by touching it, the response is again frictional with maximum force $F_f$; then, a second hardening phase after the displacement $d_1$ is present due to the involvement of a larger portion of wall, until it is damaged and the peak $F_{max}$ is reached.
This constitutive law was defined separately for quasi-static and dynamic tests, and a difference in the response is present, as will be highlighted later. This model was derived from the backbones of the obtained cycles, by considering the behaviour which would occur without damage in the wall (red dashed backbone of Figure 33): this response may still take place, as observed for sample B-QS-3 [1], and larger displacements are reached. In this way, a conservative model in terms of strength and stiffness can be formulated. The procedure for the definition of the constitutive law is summarized as follows:

1. The average frictional force $F_f$ was calculated from the test results (separately for quasi-static and dynamic tests);
2. The backbones of the positive branch were interpolated by means of a $6^{th}$ degree equation which could properly capture the initial stiffness $K_0$ and the post-frictional stiffness $K_1$.
3. Post-frictional displacement $d_1$ is identified from observation of test results;
4. The average peak force for the positive branch $F_{max}$ was calculated from the test results;
5. With the previously calculated parameters the model curve could be defined and its correlation with the experimental results was verified by means of the $R^2$ coefficient.
6. Ductility is determined as the ratio between the ultimate displacement and the yielding one, corresponding to $-F_f$ for the negative branch, and to $F_{max}$ for the positive one.

Table 3 reports the parameters adopted for the proposed constitutive law and the graphs showing its comparison with the experimental points are reported in Figures 35 to 38. Each figure shows the positive or negative data points of the 3 tests of that type. Figure 39 shows the comparison of the two models separately derived for quasi-static and dynamic tests.

Table 3 - Parameters adopted for the proposed constitutive law

| Parameter | Quasi-static test | Dynamic test |
|---|---|---|
| Frictional force $F_f$ (kN) | 1.10 | 1.00 |
| Initial stiffness $K_0$ (kN/mm) | 2.45 | 1.28 |
| Post-frictional displacement $d_1$ (mm) | 2.00 | 3.00 |
| Post-frictional stiffness $K_1$ (kN/mm) | 1.48 | 0.34 |
| Peak force $F_{max}$ (kN) | 5.75 | 3.56* |
| $R^2$ for positive branch (pulling) | 0.91 | 0.70 |
| $R^2$ for negative branch (pushing) | 0.78 | 0.70 |
| Ductility μ (pulling) | 1.83 | 1.07 |
| Ductility μ (pushing) | 22.38 | 41.9 |

* This value did not correspond to the total failure of the connection, but to the maximum load obtained by applying the maximum actuator's stroke to the joint during the dynamic test.

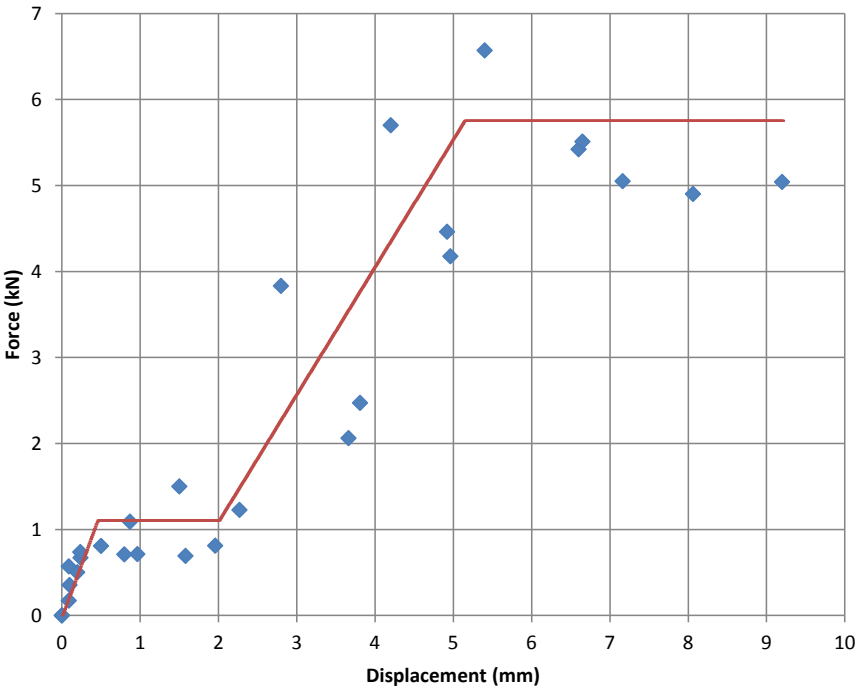


Figure 35 – Positive branch of the constitutive law compared to experimental points for quasi-static tests.

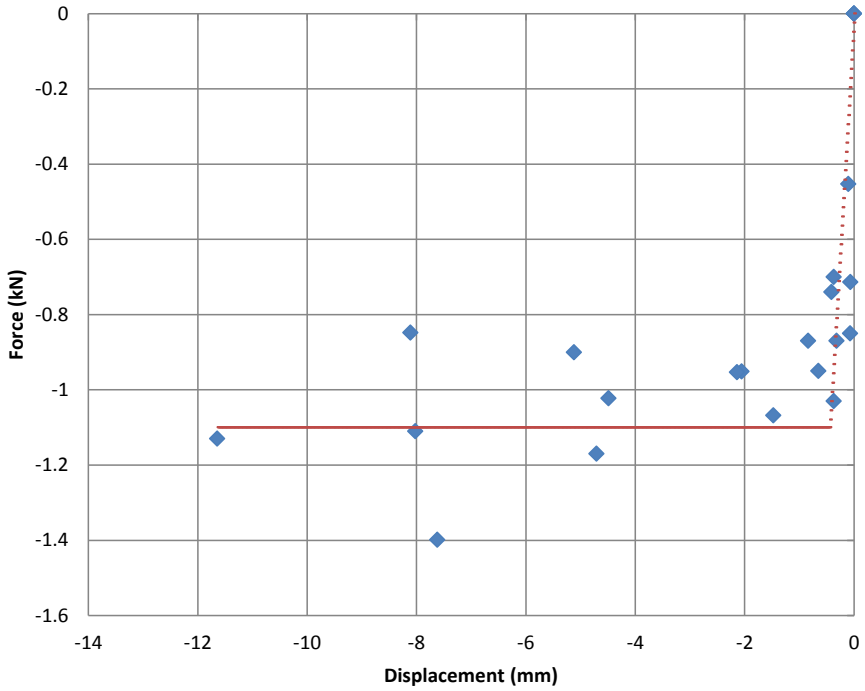


Figure 36 – Negative branch of the constitutive law compared to experimental points for quasi-static tests

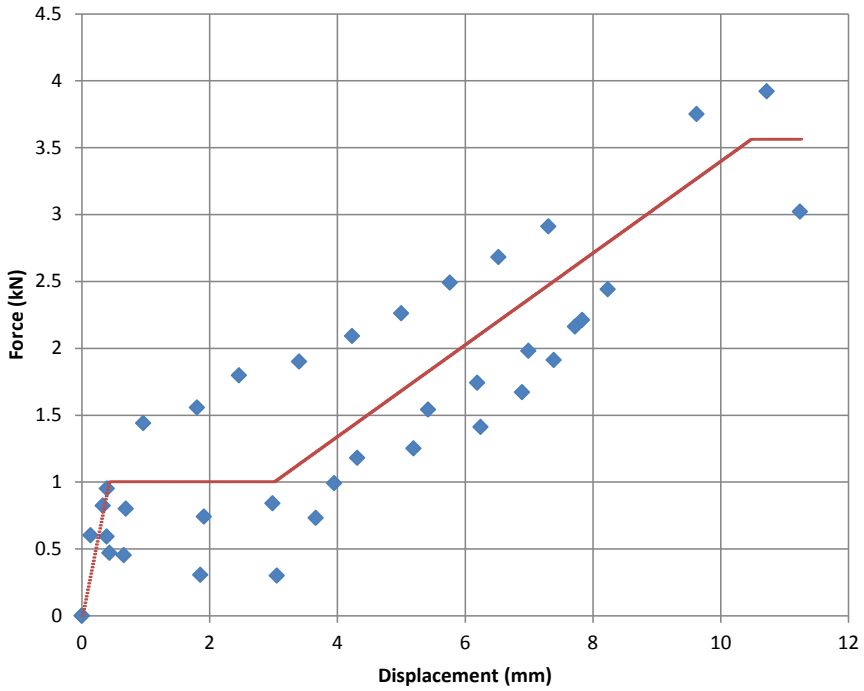


Figure 37 – Positive branch of the constitutive law compared to experimental points for dynamic tests

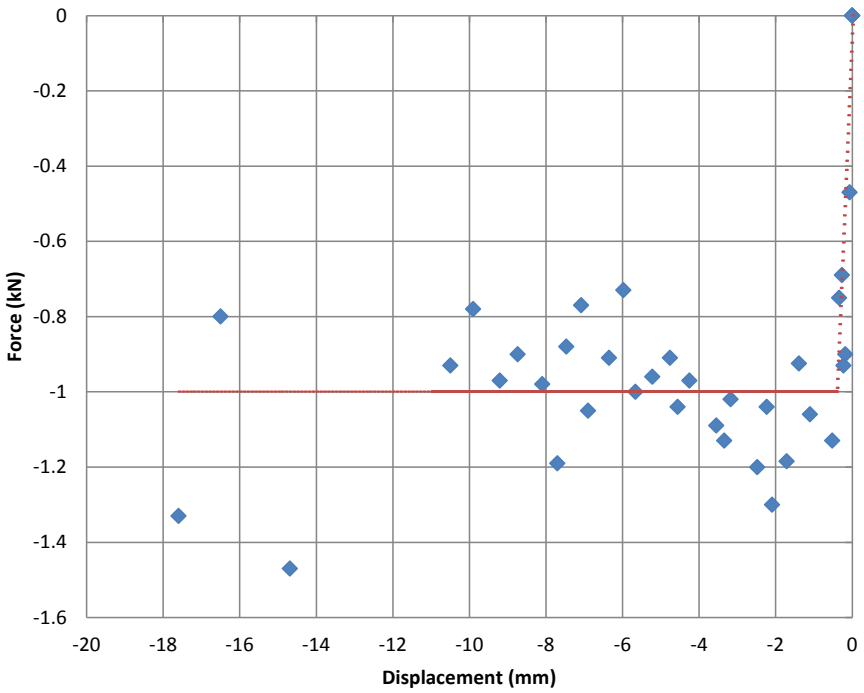


Figure 38 – Negative branch of the constitutive law compared to experimental points for dynamic tests

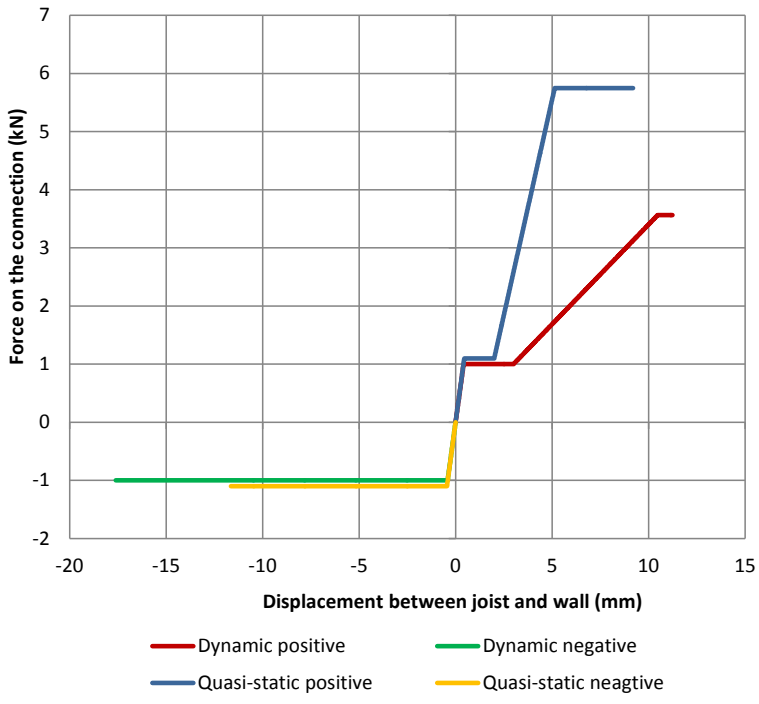


Figure 39 – Comparison between the two constitutive laws for quasi-static and dynamic tests

To conclude, the defined models appear to be well correlated to the test results and can capture the response of the hook anchor. However, the different response when the connection is subjected to dynamic loading has to be considered: while the initial stiffness is approximately the same, the remaining part of the response is much more flexible, due to the higher play present in the connection caused by the sudden loading. This corresponds to a larger value of displacement $d_1$ and a much reduced post-frictional stiffness $K_1$ for dynamic tests, and explains also the lower maximum force recorded. This value is thus not corresponding to the complete failure of the sample, but only to the load that could be reached by applying the maximum displacement from the hydraulic actuator to the wall.
Therefore, the estimation of the final resistance was correctly achieved by means of the quasi-static tests, which could lead the connection to failure; with dynamic tests these peak forces could not be reached due to the much less stiff response, which thus appears to be more conservative when defining the constitutive laws. As a last consideration, ductility is high only in the pushing direction, where frictional behaviour is involved, but similarly to configuration A, this corresponds to very low values of strength.

### 3.3.4 Configuration C

Configuration C consisted of a strengthened connection: a Rothoblaas steel angle was fastened to the wall by means of Fischer mechanical anchors and screwed to the joist.
A large improvement in strength and stiffness of the connection, compared to configurations A and B, was achieved, because it was possible to involve a large portion of the wall in the resisting process. Moreover, high values of forces were reached already for very limited displacements, thus the simultaneous movement of wall and joist was achieved as a first step against out-of-plane collapse of the wall in practice.
After the peak, the connection still exhibited displacement capacity, especially when pulling, due to the sliding of the anchors and the progressive increase of the play of the steel angle. When pushing, the joist was hitting the wall by means of the steel angle and therefore higher forces were reached, especially in the dynamic tests, where the loads were applied suddenly and an impact effect was noticed.
In any case, the walls were part of the resisting process in both directions, as shown in Figure 40.
Similarly to what was already performed for configurations A and B, a simplified bilinear model was developed to describe the response of the connection. In this case, the separation between quasi-static and dynamic tests did not lead to significant differences in terms of stiffness, but only the strength changed for the pushing direction, due to the higher values recorded during the dynamic tests.

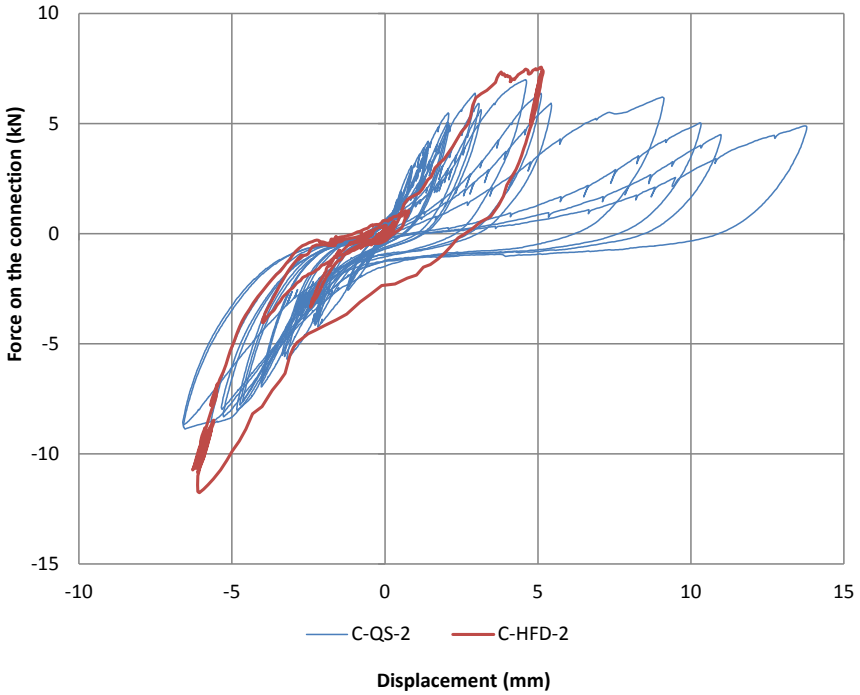


Figure 40 – Out-of-plane displacement of the wall for quasi-static and dynamic tests: in both cases, the wall is involved in the resisting process.
The procedure for the definition of the constitutive law is summarized as follows:

1. The backbones of both positive and negative branches were interpolated by means of parabolic trendlines which could properly capture both the initial stiffness and the global behaviour of the connection.
2. The area underlying the trendline was calculated, and an energy equivalent bilinear curve was derived following the same procedure as in a pushover analysis; the point at $0.6F_u$ determines the initial stiffness, and this simplified curve can well represent ductility, since it is calculated from an energy equivalence. This calculation was performed separately for quasi-static and dynamic tests.
3. After determining the parameters of the bilinear curve, its correlation with the experimental results was verified by means of the $R^2$ coefficient.
4. Ductility was calculated for the bilinear curves derived from quasi-static and dynamic tests.

Table 4 reports the parameters adopted for the proposed constitutive law and the graphs showing its comparison with the experimental points are reported in Figures 41 to 44. Figure 45 shows the comparison of the two models separately derived for quasi-static and dynamic tests.

Table 4 - Parameters calculated for the proposed constitutive law

| Parameter | Quasi-static test | Dynamic test |
|---|---|---|
| Initial stiffness $K_0$ (kN/mm) | 4.19 | 4.37 |
| Peak force (+) $F_{max}$ (kN) | 6.37 | 6.69 |
| Peak force (-) $F_{max}$ (kN) | 9.40 | 14.09 |
| $R^2$ for positive branch (pulling) | 0.93 | 0.78 |
| $R^2$ for negative branch (pushing) | 0.93 | 0.93 |
| Ductility μ (pulling) | 2.68 | 10.48 |
| Ductility μ (pushing) | 2.34 | 2.09 |

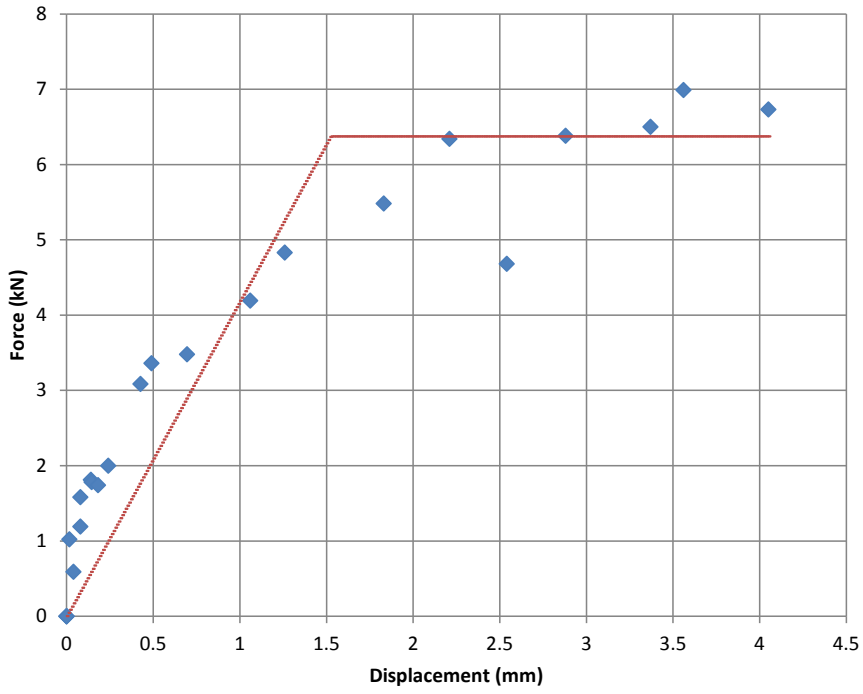


Figure 41 – Positive branch of the constitutive law compared to experimental points for quasi-static tests.

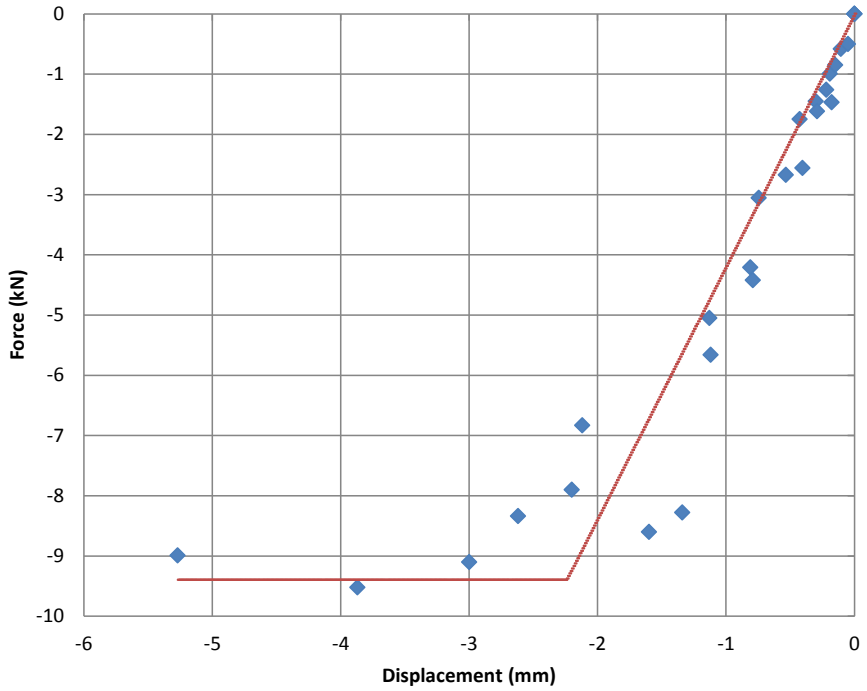


Figure 42 – Negative branch of the constitutive law compared to experimental points for quasi-static tests

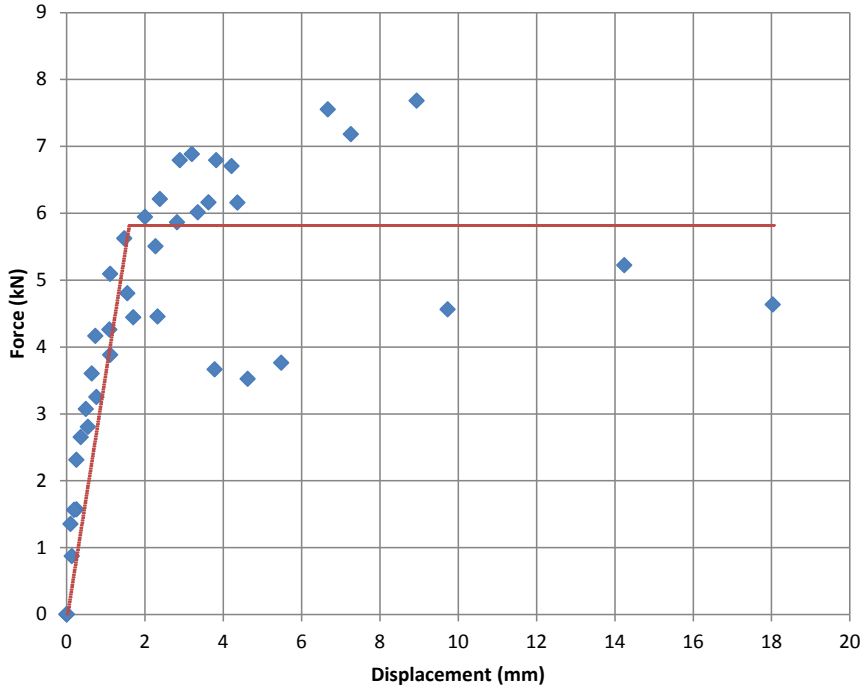


Figure 43 – Positive branch of the constitutive law compared to experimental points for dynamic tests

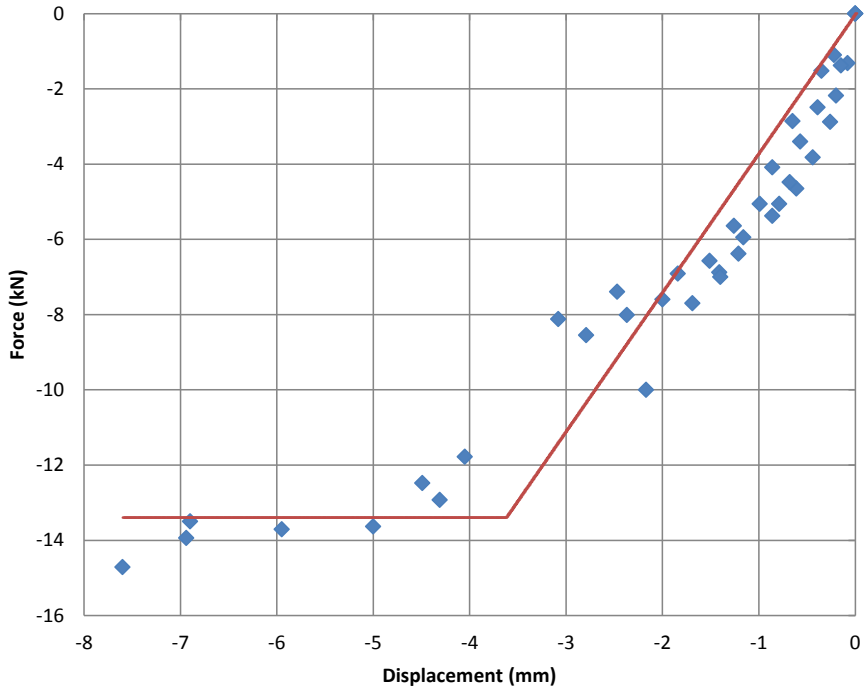


Figure 44 – Negative branch of the constitutive law compared to experimental points for dynamic tests

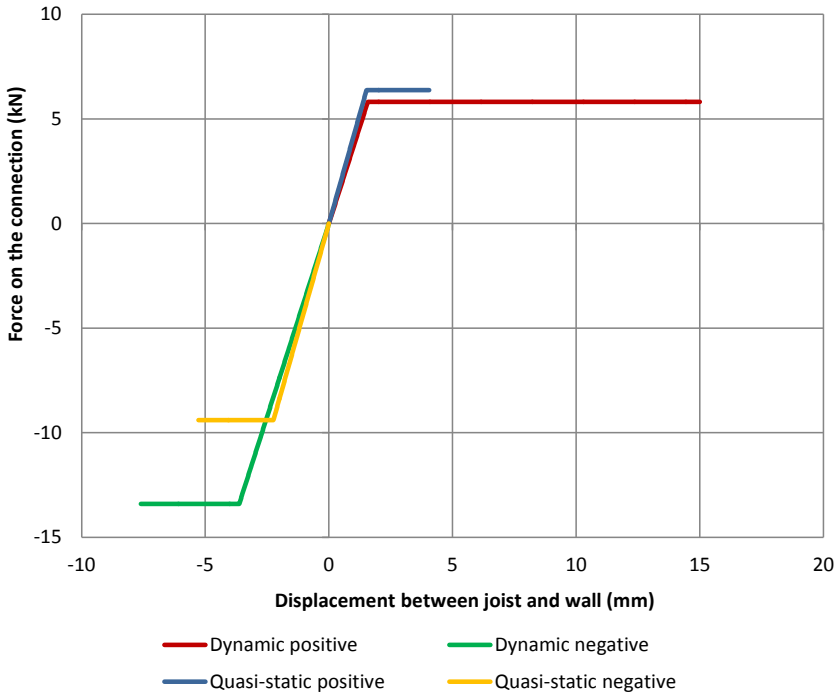


Figure 45 – Comparison between the two constitutive laws for quasi-static and dynamic tests

From the obtained curves, the defined models appear to be well correlated to the test results and can capture correctly the response of this strengthened connection. In this case the behaviour can be considered much more similar between quasi-static and dynamic tests, because the only difference is in the impact effect leading to higher values of strength when pushing. As for pulling, since in both cases the resistance is related to the extraction of the anchors, similar values were obtained. Finally, from quasi-static tests it is possible to properly capture the properties of the connection in a safe way: this is also visible for ductility, because in dynamic tests this was much higher for pulling direction.

### 3.3.5 Configuration D

Configuration D consisted of a strengthened connection as well: an additional joist placed below the existing one was fastened to the wall by means of Fischer mechanical anchors and the two joists were connected to each other with two steel brackets screwed on them.
An improvement in strength and stiffness of the connection was achieved, because it was possible to involve a large portion of the wall in the resisting process. Moreover, high values of forces were reached already for very limited displacements, thus the simultaneous movement of wall and joist was achieved as a first step against out-of-plane collapse of the wall in practice.
The connection exhibited in general displacement capacity, due to rotation, bending and yielding of the steel brackets and the screws. For large displacements, one of the two anchors exhibited pull-out failure leading to a drop in the resistance of the connection. Since the initial response of the connection was mainly influenced by the play of the brackets and the screws, large dispersion in the test results was observed according to when rotation or yielding were starting to take place. Another aspect is related, like in configuration B, to the difficulty in extrapolating backbone curves for large displacements, because the cycles were influenced by the damage of the wall: they were therefore either centred with respect to the origin of the axes, or not considered when the response was not clear. This issue never occurred for the initial and more important phases.
In any case, the connection was able to involve a large portion of the walls, which were part of the resisting process in both directions, as shown in Figure 46, and for quasi-static and dynamic tests in the same measure.
Similarly to what was already performed for configurations A, B and C a simplified bilinear model was developed to describe the response of the connection. In this case, the separation between quasi-static and dynamic tests did not lead to significant differences in terms of stiffness, but only the strength changed for the pulling direction, due to the higher values recorded during the quasi-static tests.

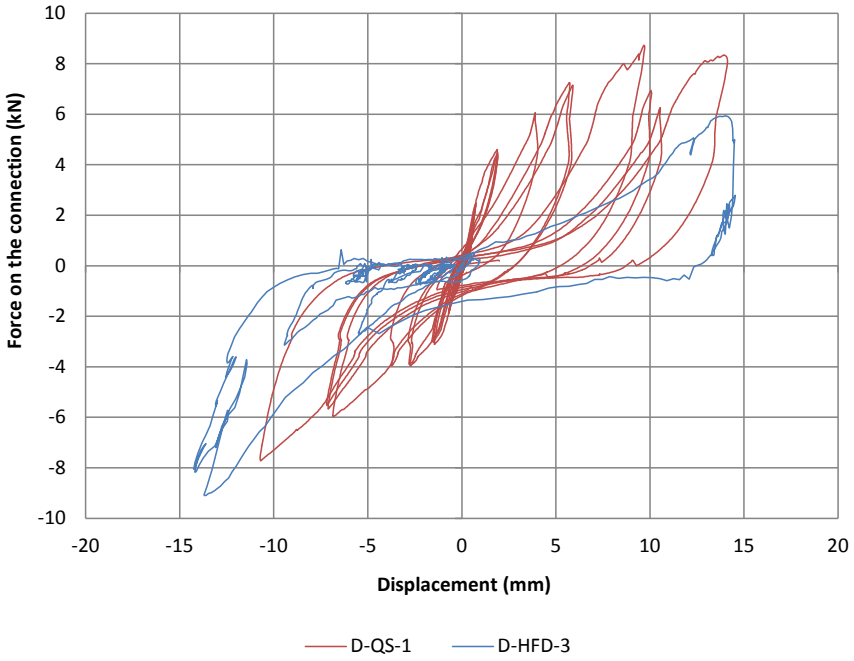


Figure 46 – Out-of-plane displacement of the wall for quasi-static and dynamic tests: in both cases, the wall is involved in the resisting process

The procedure for the definition of the constitutive law is summarized as follows:

1. The backbones of both positive and negative branches were interpolated by means of parabolic trendlines which could properly capture both the initial stiffness and the global behaviour of the connection.
2. The area underlying the trendline was calculated, and an energy equivalent bilinear curve was derived following the same procedure as in a pushover analysis; the point at $0.6F_u$ determines the initial stiffness, and this simplified curve can well represent ductility, since it is calculated from an energy equivalence. This calculation was performed separately for quasi-static and dynamic tests.
3. After determining the parameters of the bilinear curve, its correlation with the experimental results was verified by means of the $R^2$ coefficient.
4. Ductility was calculated for the bilinear curves derived from quasi-static and dynamic tests.

Table 5 reports the parameters adopted for the proposed constitutive law and the graphs showing its comparison with the experimental points are reported in Figures 47 to 50. Figure 51 shows the comparison of the two models separately derived for quasi-static and dynamic tests.

Table 5 - Parameters calculated for the proposed constitutive law

| Parameter | Quasi-static test | Dynamic test |
|---|---|---|
| Initial stiffness $K_0$ (kN/mm) | 2.26 | 1.74 |
| Peak force (+) $F_{max}$ (kN) | 7.55 | 4.46 |
| Peak force (-) $F_{max}$ (kN) | 6.97 | 10.09 |
| $R^2$ for positive branch (pulling) | 0.78 | 0.62 |
| $R^2$ for negative branch (pushing) | 0.71 | 0.84 |
| Ductility μ (pulling) | 1.99 | 4.51 |
| Ductility μ (pushing) | 2.96 | 1.94 |

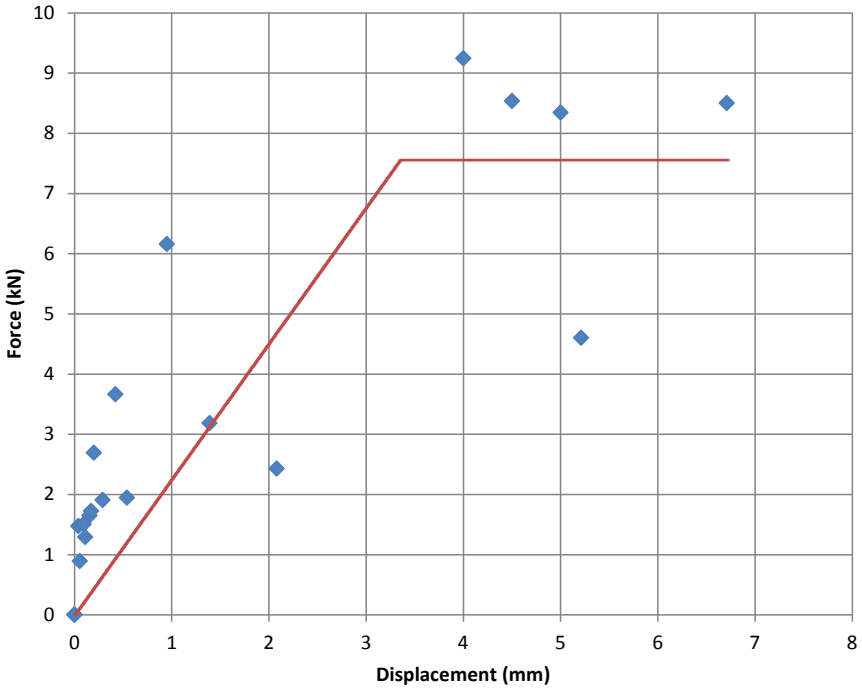


Figure 47 – Positive branch of the constitutive law compared to experimental points for quasi-static tests

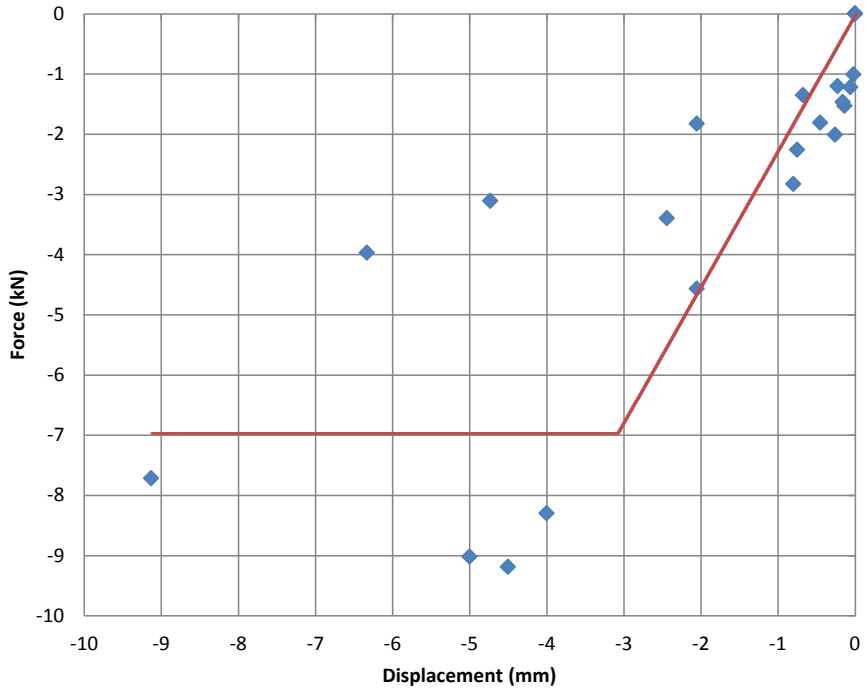


Figure 48 – Negative branch of the constitutive law compared to experimental points for quasi-static tests

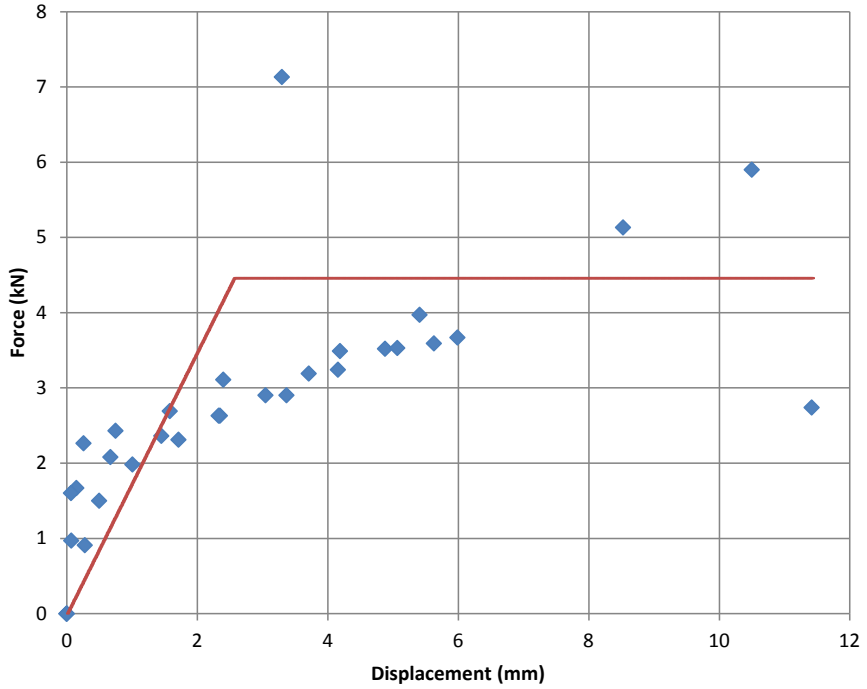


Figure 49 – Positive branch of the constitutive law compared to experimental points for dynamic tests

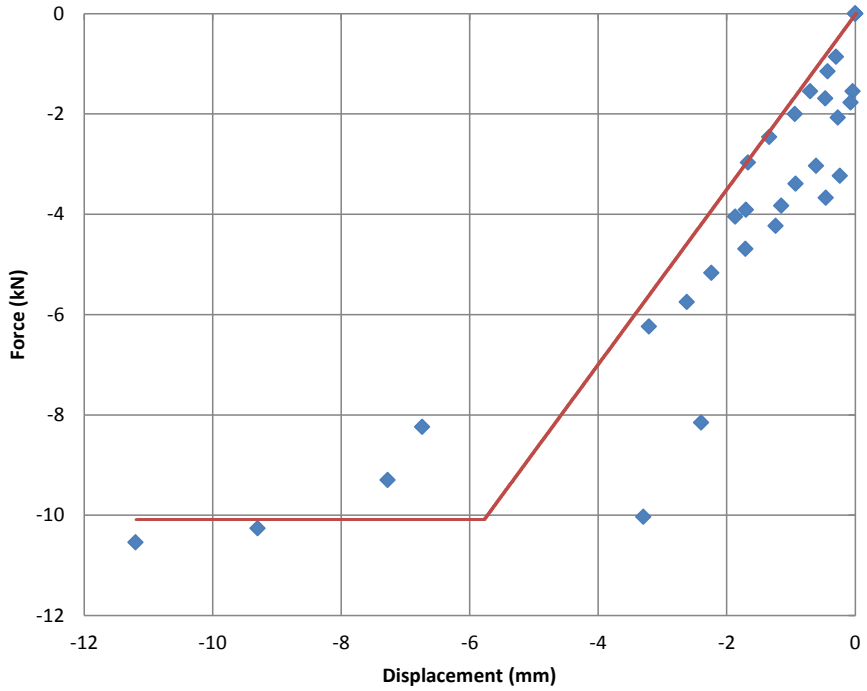


Figure 50 – Negative branch of the constitutive law compared to experimental points for dynamic tests

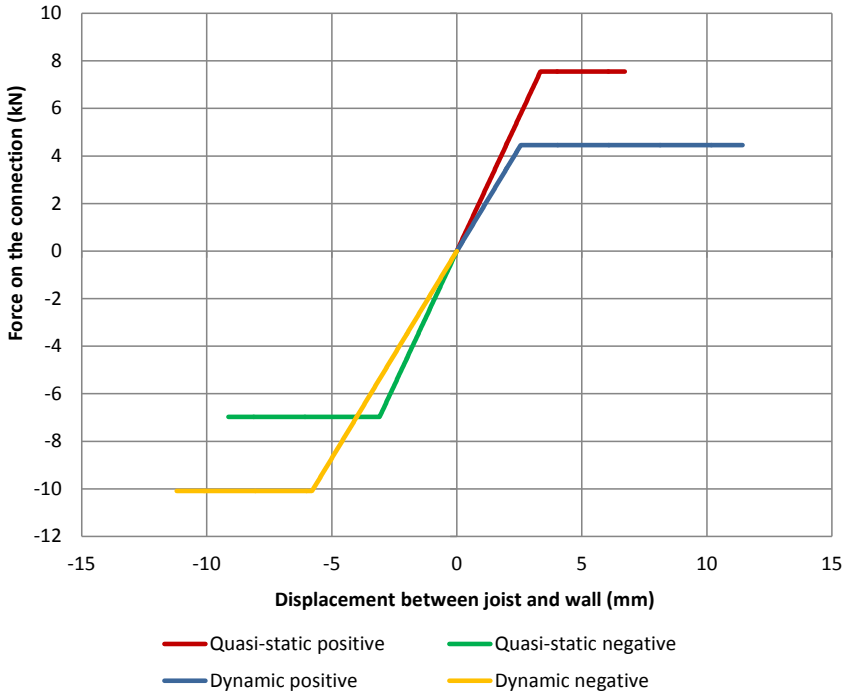


Figure 51 – Comparison between the two constitutive laws for quasi-static and dynamic tests

From the obtained curves, although the dispersion of data was wider if compared to the previous cases, the defined models appear to be sufficiently correlated to the test results and can capture correctly the response of this strengthened connection. It should be noticed that for this configuration also an elastoplastic-hardening bilinear curve could be suitable to represent its behaviour.
The response is similar for quasi-static and dynamic loading, except for the strength of the connection when pulling: this is lower for dynamic loading probably because of the higher play (and ductility) induced in the joint due to suddenly applied forces. The stiffness appears instead to be very similar between the two test types. The opposite happened for the pushing direction, again due to the impact effect, which reduced also the ductility. In any case, the deformation on the steel brackets was always preceding the extraction of the anchors, which occurred at the very last runs during the test.

### 3.3.6 Configuration E

Configuration E also consisted of a strengthened connection: a traditional hook anchor was nailed to the joist and embedded in an incision filled with epoxy in the masonry wall.
An improvement in strength and stiffness of the connection was achieved, because it was possible to involve a large portion of the wall in the resisting process, especially when pushing. In comparison to the other tested configurations, this one exhibited a more brittle behaviour in pulling, due to the cracking of the masonry around the epoxy, leading to the detachment of the hook anchor.
This detachment influenced the response at most, because the pulling strength depended on this brittle failure mode, causing dispersion in the results. Instead, in the pushing direction, the behaviour was more constant for the various samples, which showed displacement capacity and ductility as well. This was mainly related to damage and cracks on the wall. Until the detachment of the hook anchor, the connection was capable of involving the whole wall in the resisting process, and this was observed for both cyclic and dynamic tests (Figure 52). After the detachment, this behaviour was noticed only in the pushing direction: this is clearly visible from Figure 52, because at an amplitude of 5 mm the wall is involved in both directions during the dynamic test, while at a larger amplitude of 10 mm only in pushing the strength of the wall is activated.
Similarly to previous cases, a simplified bilinear model was developed to describe the response of the connection. The principle of energy equivalence is now adopted only for the pushing direction, while for the pulling one a bilinear curve with softening was better representing the response of the joint.

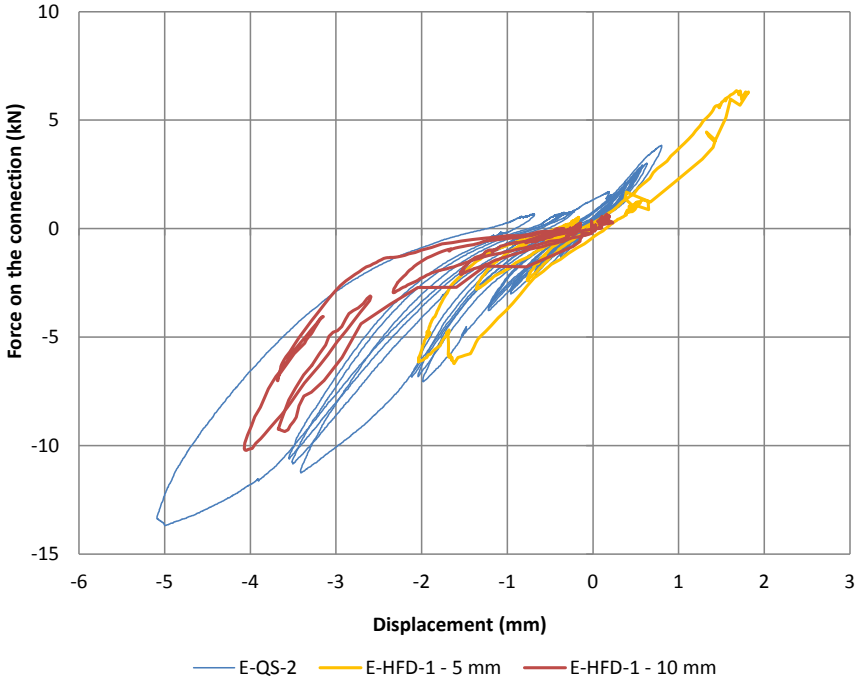


Figure 52 – Out-of-plane displacement of the wall for quasi-static and dynamic tests: in both cases, the wall is involved in the resisting process, but in the pulling direction only until detachment of the hook anchor.

The procedure for the definition of the constitutive law is summarized as follows:

1. The backbones of negative branches were interpolated by means of parabolic trendlines which could properly capture both the initial stiffness and the global behaviour of the connection.
2. The area underlying the trendline was calculated, and an energy equivalent bilinear curve was derived following the same procedure as in a pushover analysis; the point at $0.6F_u$ determines the initial stiffness, and this simplified curve can well represent ductility, since it is calculated from an energy equivalence. This calculation was performed separately for quasi-static and dynamic tests.
3. After determining the parameters of the bilinear curve, its correlation with the experimental results was verified by means of the $R^2$ coefficient.
4. Ductility was calculated for the bilinear curves derived from quasi-static and dynamic tests, only for the non-brittle direction (pushing).
5. The backbones of positive branches were interpolated with a bilinear trendline with softening, and their correlation to experimental results was verified by means of the $R^2$ coefficient.

Table 6 reports the parameters adopted for the proposed constitutive law and the graphs showing its comparison with the experimental points are reported in Figures 53 to 56. Figure 57 shows the comparison of the two models separately derived for quasi-static and dynamic tests.

Table 6 - Parameters calculated for the proposed constitutive law

| Parameter | Quasi-static test | Dynamic test |
|---|---|---|
| Initial stiffness $K_0$ (kN/mm) | 12.85 | 10.38 |
| Peak force (+) $F_{max}$ (kN) | 4.42 | 5.33 |
| Peak force (-) $F_{max}$ (kN) | 12.77 | 14.23 |
| $R^2$ for positive branch (pulling) | 0.75 | 0.73 |
| $R^2$ for negative branch (pushing) | 0.76 | 0.75 |
| Post-yielding stiffness $K_1$ (kN/mm) (pulling) | -0.31 | -0.35 |
| Ductility μ (pushing) | 7.42 | 7.35 |

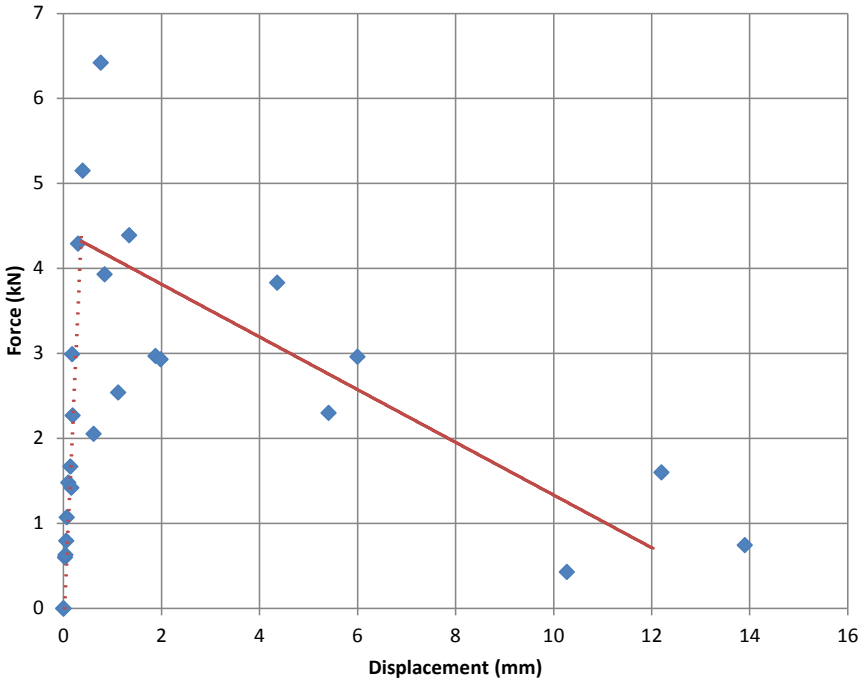

Figure 53 – Positive branch of the constitutive law compared to experimental points for quasi-static tests

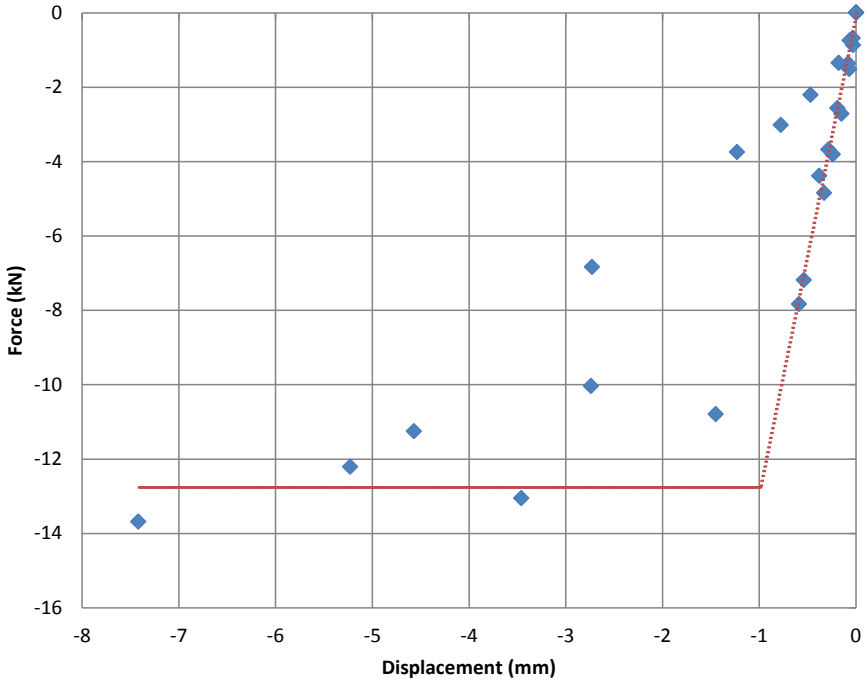


Figure 54 – Negative branch of the constitutive law compared to experimental points for quasi-static tests

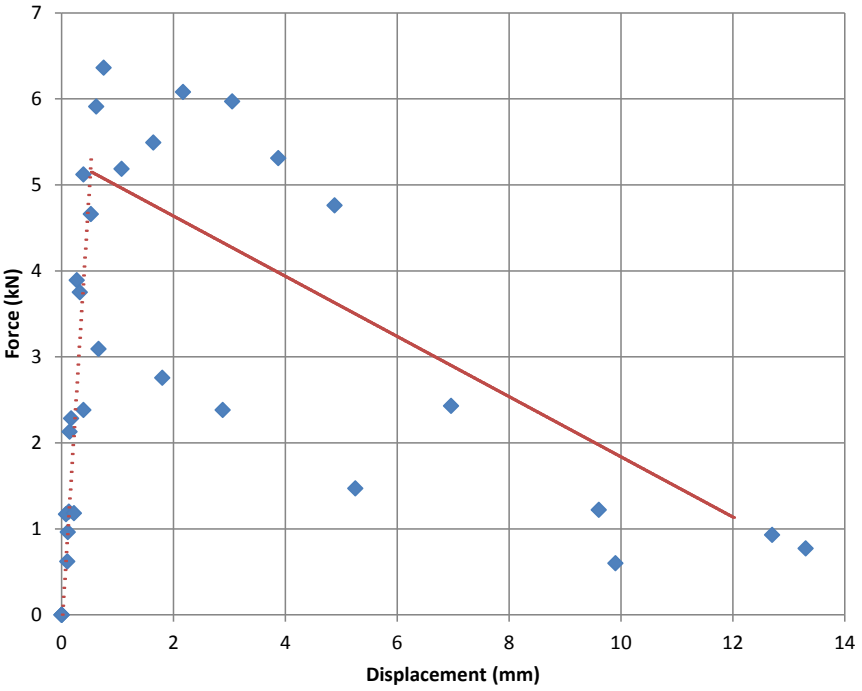


Figure 55 – Positive branch of the constitutive law compared to experimental points for dynamic tests

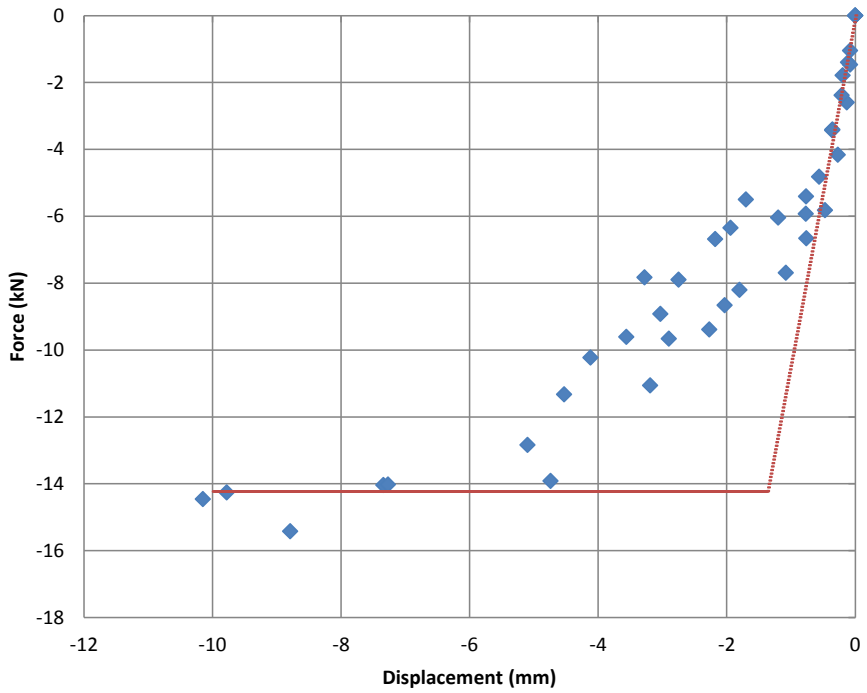


Figure 56 – Negative branch of the constitutive law compared to experimental points for dynamic tests

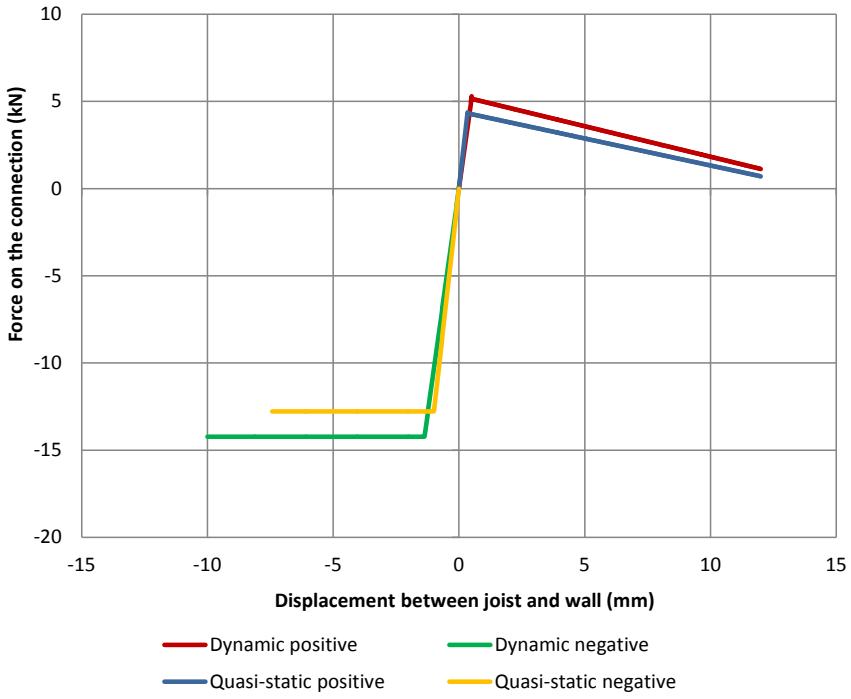


Figure 57 – Comparison between the two constitutive laws for quasi-static and dynamic tests

From the obtained curves, the defined constitutive laws appear to be sufficiently correlated to the test results and can capture correctly the response of this strengthened connection. The behaviour is in this case very similar for quasi-static and dynamic loading, in terms of both ductility (pushing direction) and peak and post-peak phase (pulling direction). Quasi-static tests proved to be representative and to provide a good estimation of the actual strength and stiffness reached during dynamic loading.

### 3.3.7 Configuration F

Configuration F also consisted of a strengthened joint: screws were connecting the joist to the wall, in which holes were drilled and filled with epoxy.
A significant improvement in strength and stiffness of the connection was achieved, because it was possible to involve a large portion of the wall within a very limited displacement between this and the joist.
The failure was mainly related to cracks and damage to the masonry, while the screws did not detach from the epoxy layer, which in turn remained always anchored to the wall.
For both cyclic and dynamic tests the walls could reach large out-of-plane displacements because of the effective connection with the joist (Figure 58).
Similarly to previous cases, a simplified bilinear model was developed to describe the response of the connection, by adopting again the principle of energy equivalence.
The procedure for the definition of the constitutive law is summarized as follows:

1. The backbones of both positive and negative branches were interpolated by means of parabolic trendlines which could properly capture both the initial stiffness and the global behaviour of the connection.
2. The area underlying the trendline was calculated, and an energy equivalent bilinear curve was derived following the same procedure as in a pushover analysis; the point at $0.6F_u$ determines the initial stiffness, and this simplified curve can well represent ductility, since it is calculated from an energy equivalence. This calculation was performed separately for quasi-static and dynamic tests.
3. After determining the parameters of the bilinear curve, its correlation with the experimental results was verified by means of the $R^2$ coefficient.
4. Ductility was calculated for the bilinear curves derived from quasi-static and dynamic tests.

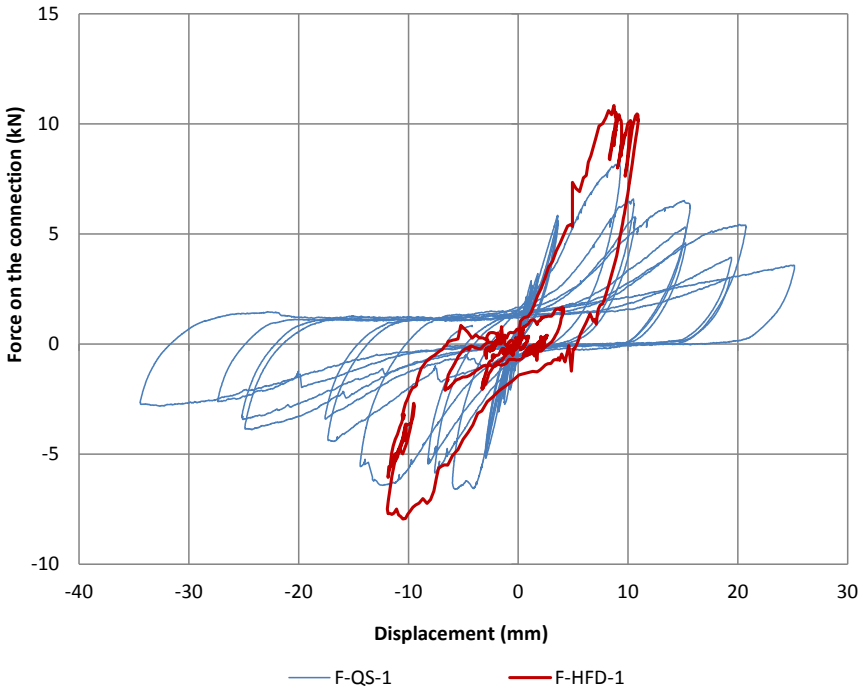


Figure 58 – Out-of-plane displacement of the wall for quasi-static and dynamic tests: in both cases, the wall is fully involved in the resisting process.

Table 7 reports the parameters adopted for the proposed constitutive law and the graphs showing its comparison with the experimental points are reported in Figures 59 to 62. Figure 63 shows the comparison of the two models separately derived for quasi-static and dynamic tests.

Table 7 - Parameters calculated for the proposed constitutive law

| Parameter | Quasi-static test | Dynamic test |
|---|---|---|
| Initial stiffness $K_0$ (kN/mm) | 7.94 | 5.35 |
| Peak force (+) $F_{max}$ (kN) | 8.52 | 11.65 |
| Peak force (-) $F_{max}$ (kN) | 6.25 | 8.67 |
| $R^2$ for positive branch (pulling) | 0.77 | 0.91 |
| $R^2$ for negative branch (pushing) | 0.75 | 0.78 |
| Ductility μ (pulling) | 3.14 | 1.69(1) |
| Ductility μ (pushing) | 4.94 | 3.99(2) |

(1) This value of ductility refers to the proposed bilinear curve, which however does not represent the whole amount of data points: it was chosen to derive it only for the data points that were common to all the three performed dynamic tests. For two of them, the reached ultimate displacement was higher and the ductility that they exhibited was around the value of 3.5, therefore in line with what obtained for quasi-static tests.

(2) As explained for the pulling direction, only two dynamic tests showed higher ultimate displacements and a ductility value very similar to what obtained for quasi-static tests. Since this was not obtained for all the tests, it was chosen not to include the data point with too large displacement to have a coherent representation of the load-slip behaviour through the bilinear curve.

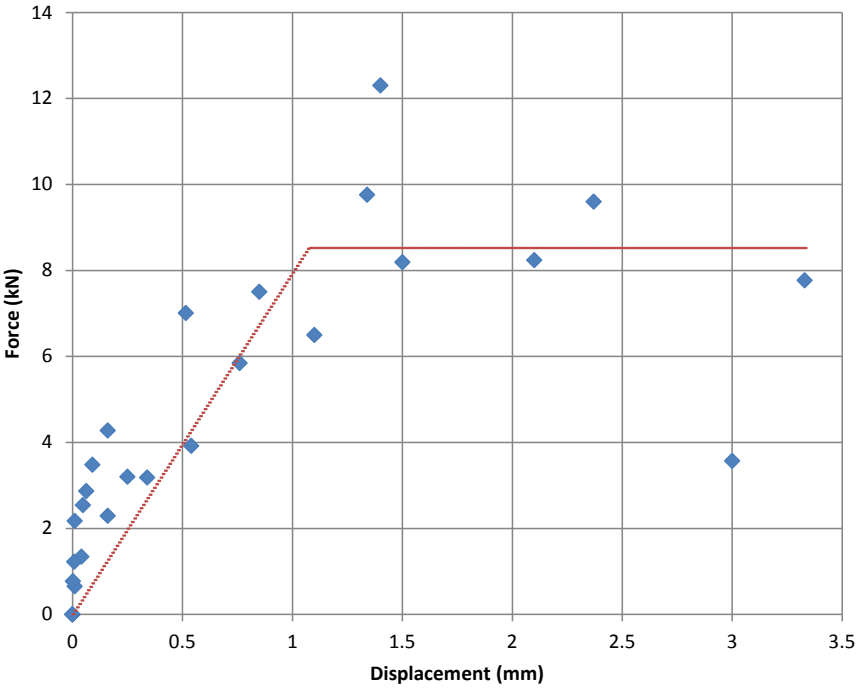


Figure 59 – Positive branch of the constitutive law compared to experimental points for quasi-static tests

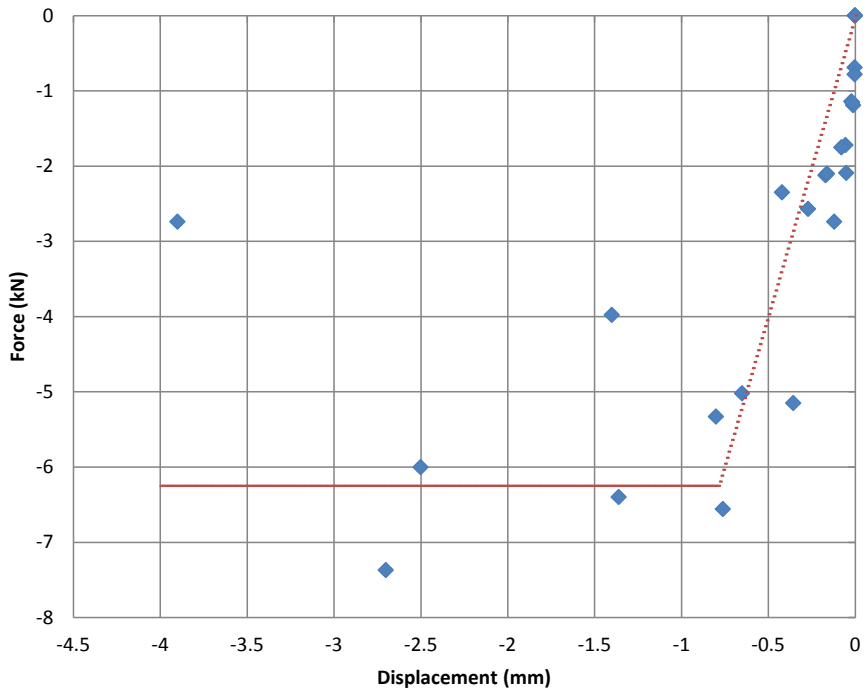


Figure 60 – Negative branch of the constitutive law compared to experimental points for quasi-static tests

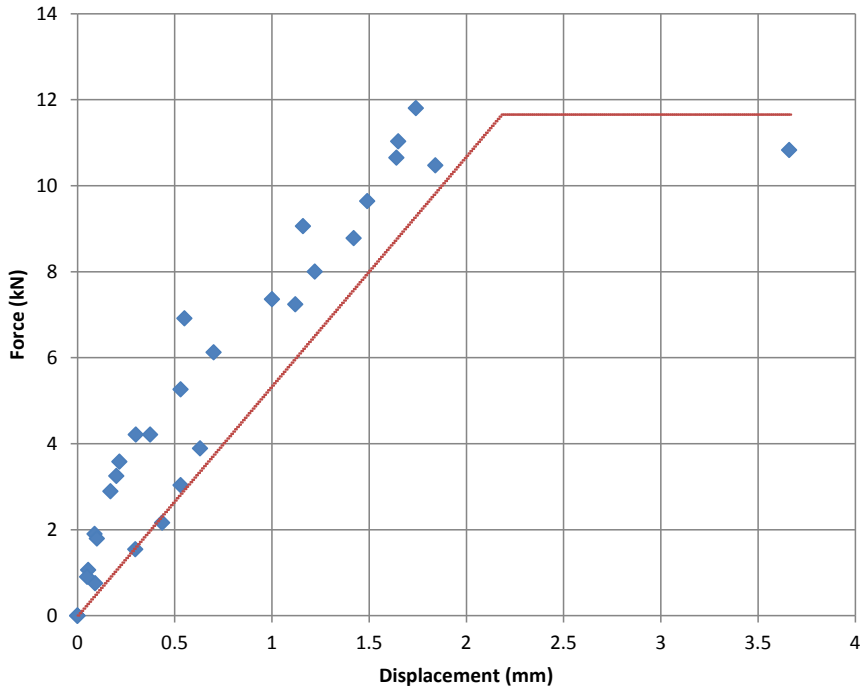


Figure 61 – Positive branch of the constitutive law compared to experimental points for dynamic tests

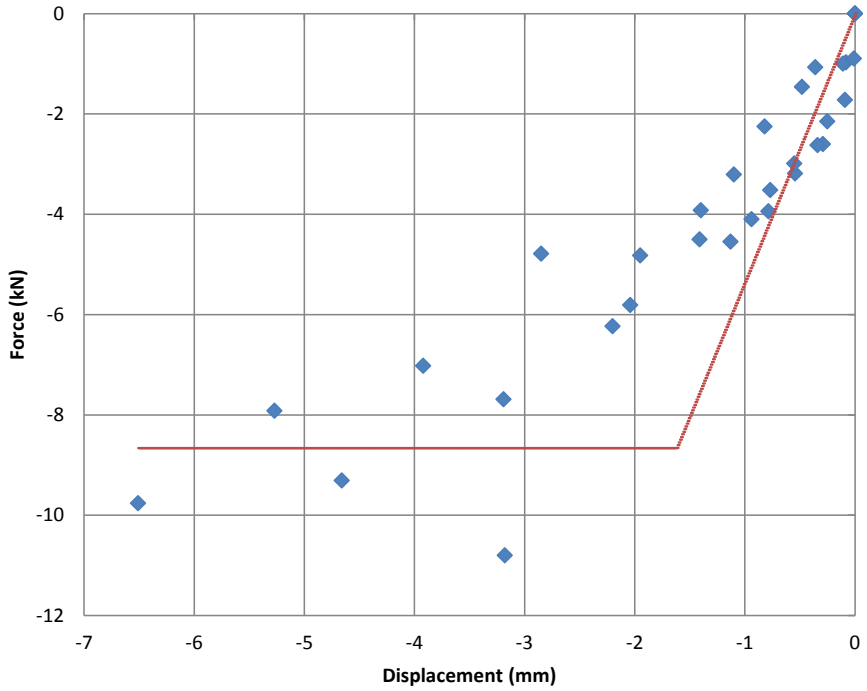


Figure 62 – Negative branch of the constitutive law compared to experimental points for dynamic tests

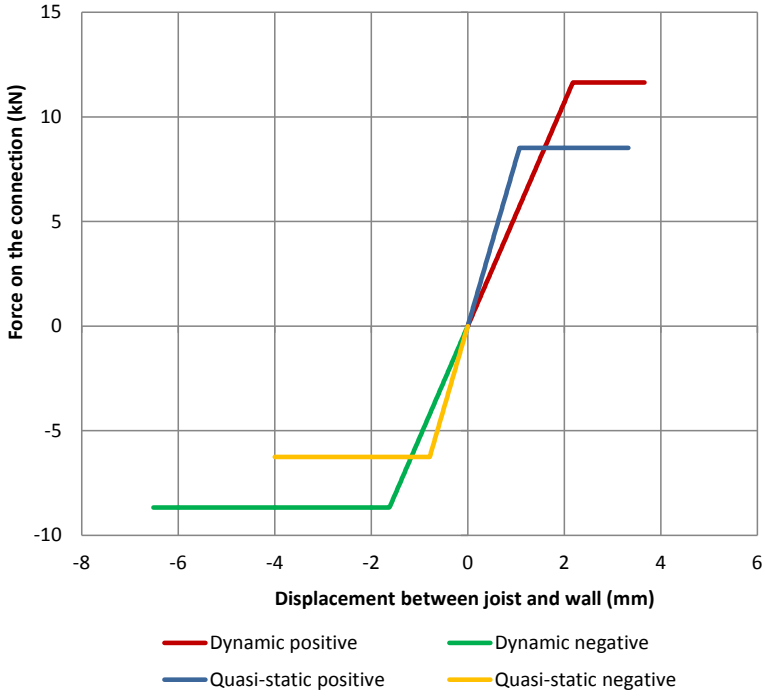


Figure 63 – Comparison between the two constitutive laws for quasi-static and dynamic tests

From the obtained curves, the defined constitutive laws appear to be well correlated to the test results and can correctly capture the response of this strengthened connection. It is interesting to notice that, due to the very stiff joint, in this case the impact effect is present also for the pulling direction, while in the previous strengthened configurations it was observed only for the pushing one. Conversely, the stiffness appeared to be lower, probably because the suddenly applied load resulted in a slightly higher play in the screws. The response determined with quasi-static cyclic test is again a safe estimation of the actual dynamic behaviour.

### 3.3.8 Configuration G

Configuration G was the last strengthened joint tested in this campaign: timber blocks were used to connect the floor sheathing strengthened with plywood panels, the joist and the wall. Screws fastened all timber members among each other, while mechanical anchors connected the blocks to the wall.
A significant improvement in strength and stiffness of the connection was achieved, but also displacement capacity was enhanced. This was mainly related to yielding and bending of fasteners.
The failure of the samples occurred due to cracks and damage to the masonry, and in the very last phases also due to pull-out failure of some of the anchors.
For both cyclic and dynamic tests the walls could reach large out-of-plane displacements because of the effective connection with the joist (Figure 64).
Similarly to previous cases, a simplified bilinear model was developed to describe the response of the connection, by adopting again the principle of energy equivalence.

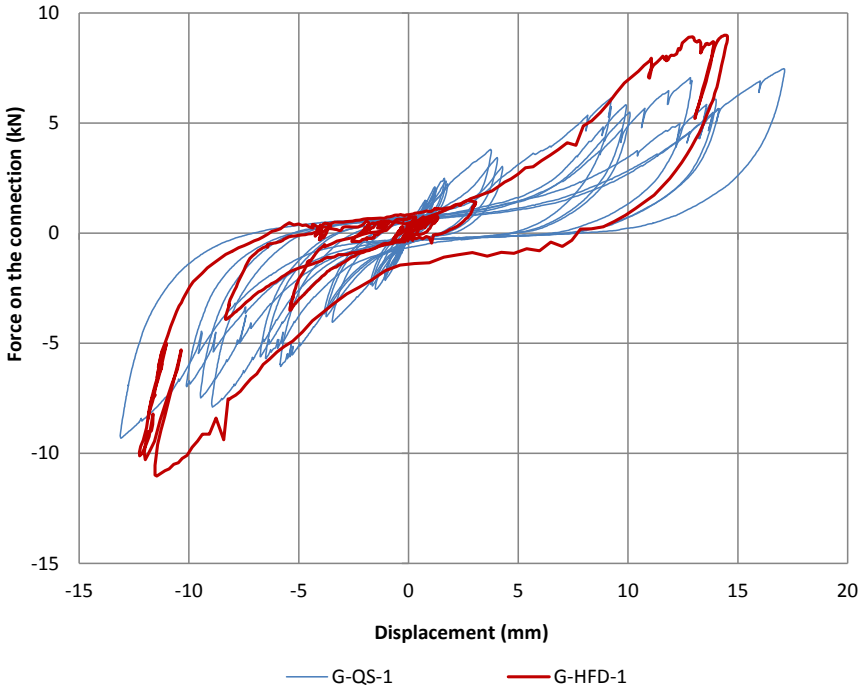


Figure 64 – Out-of-plane displacement of the wall for quasi-static and dynamic tests: in both cases, the wall is fully involved in the resisting process.

The procedure for the definition of the constitutive law is summarized as follows:

1. The backbones of both positive and negative branches were interpolated by means of parabolic trendlines which could properly capture both the initial stiffness and the global behaviour of the connection.
2. The area underlying the trendline was calculated, and an energy equivalent bilinear curve was derived following the same procedure as in a pushover analysis; the point at $0.6F_u$ determines the initial stiffness, and this simplified curve can well represent ductility, since it is calculated from an energy equivalence. This calculation was performed separately for quasi-static and dynamic tests.
3. After determining the parameters of the bilinear curve, its correlation with the experimental results was verified by means of the $R^2$ coefficient.
4. Ductility was calculated for the bilinear curves derived from quasi-static and dynamic tests.

Table 8 reports the parameters adopted for the proposed constitutive law and the graphs showing its comparison with the experimental points are reported in Figures 65 to 68. Figure 69 shows the comparison of the two models separately derived for quasi-static and dynamic tests.

Table 8 - Parameters calculated for the proposed constitutive law

| Parameter | Quasi-static test | Dynamic test |
|---|---|---|
| Initial stiffness $K_0$ (kN/mm) | 1.06 | 1.92 |
| Peak force (+) $F_{max}$ (kN) | 6.34 | 9.75 |
| Peak force (-) $F_{max}$ (kN) | 7.64 | 11.66 |
| $R^2$ for positive branch (pulling) | 0.83 | 0.90 |
| $R^2$ for negative branch (pushing) | 0.91 | 0.91 |
| Ductility μ (pulling) | 2.83 | 3.48 |
| Ductility μ (pushing) | 1.73 | 2.66 |

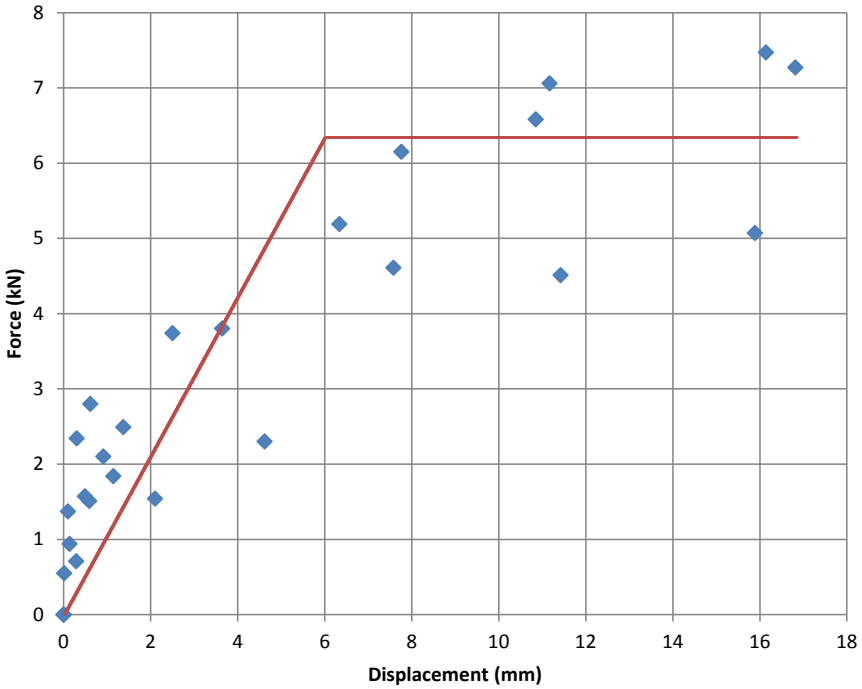


Figure 65 – Positive branch of the constitutive law compared to experimental points for quasi-static tests

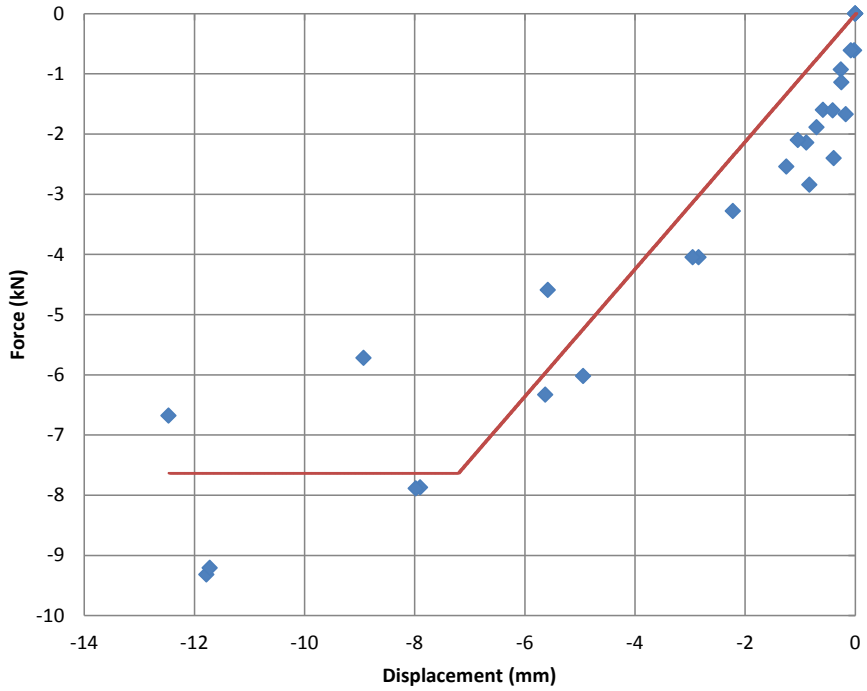


Figure 66 – Negative branch of the constitutive law compared to experimental points for quasi-static tests

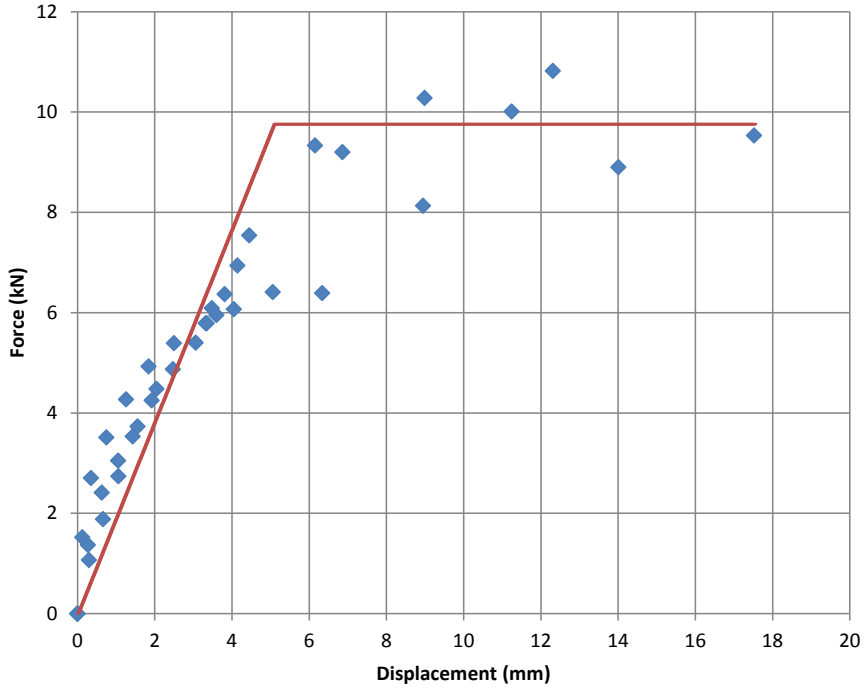


Figure 67 – Positive branch of the constitutive law compared to experimental points for dynamic tests

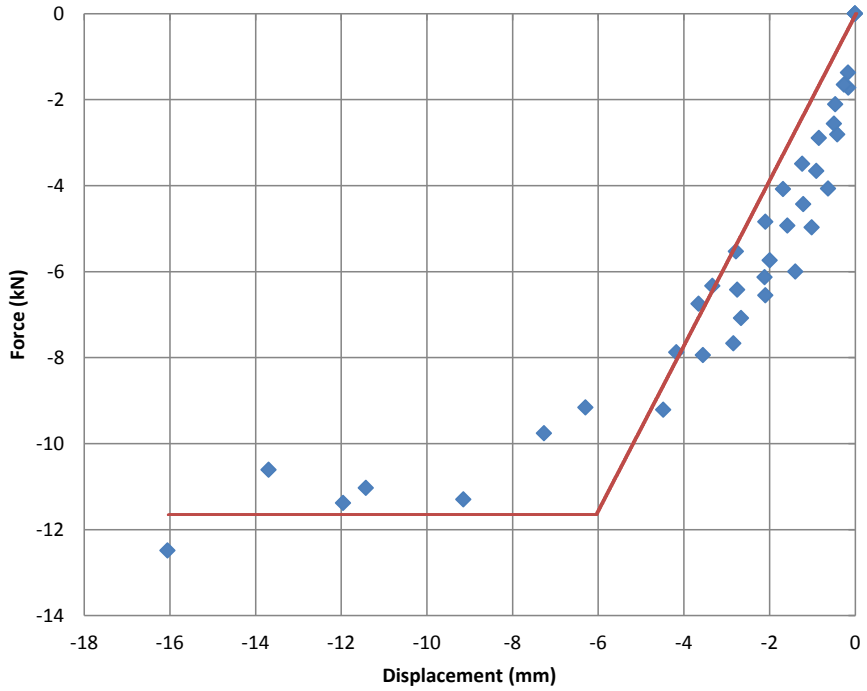


Figure 68 – Negative branch of the constitutive law compared to experimental points for dynamic tests

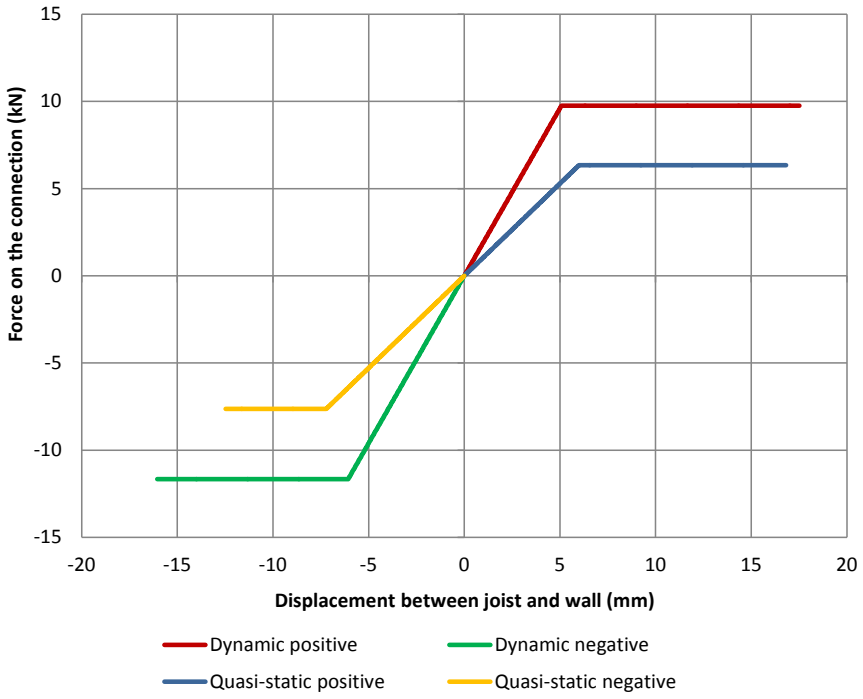


Figure 69 – Comparison between the two constitutive laws for quasi-static and dynamic tests

From the obtained curves, the defined constitutive laws appear to be very well correlated to the test results and can correctly capture the response of this strengthened connection. The response determined with quasi-static cyclic test is again a safe estimation of the actual dynamic behaviour, which in this case exhibited higher values of both strength and stiffness. The increased strength was probably due to the impact effect, which occurred in both directions. The increase in strength, instead, was probably related to the increased friction among timber members when loading them suddenly, because in this case also the fasteners are immediately brought into play compared to quasi-static tests.

## 3.4 Recommendations for calculation of strengthened joints

### 3.4.1 General

In this section, based on the obtained test results, some recommendations for the calculation of strengthened joints will be presented. The described methods are referred to both the failure modes discussed in section 3.2, and the simplified bilinear curves derived in section 3.3.

### 3.4.2 Configuration A

For configuration A, the values and frictional models described in section 3.3.2 can be adopted; they provide a safe estimation of the final strength of this joint type.

### 3.4.3 Configuration B

For configuration B, the values of strength and stiffness reported in section 3.3.3 can be adopted given the standard measure for the tested hook anchor. It is recommended, however, to account for the higher play that characterizes dynamic tests for this joints, using therefore a reduced value of stiffness based on the dynamic behaviour. In other words, the strength from quasi-static tests should be combined with the stiffness of dynamic tests, obtaining the following parameters for this modified constitutive law:

1. Pulling direction:
    - Frictional force $F_f$: 1.00 kN
    - Initial stiffness $K_0$: 1.28 kN/mm
2. Pushing direction:
    - Frictional force $F_f$: 1.00 kN
    - Initial stiffness $K_0$: 1.28 kN/mm
    - Post-frictional displacement $d_1$: 3.00 mm
    - Post-frictional stiffness $K_1$: 0.34 kN/mm
    - Peak force $F_{max}$: 5.75 kN

### 3.4.4 Configuration C

By examining the different components of this strengthened connection, the main uncertainty in the failure modes is related to the behaviour of mechanical anchors and their interaction with masonry. The screws can be calculated with the usual Johansen's model as reported in EC5 [4], while the principle of overstrength has to be applied to the steel angle. However, since only a limited number of screws connects the steel angle to the joist, the overstrength appears to be always guaranteed.
With regard to the mechanical anchors, instead, the behaviour can be influenced by either their pull-out strength, or the extraction from the wall of the bricks in which they are fastened. From performed pull-out tests on mechanical anchors [5], the average measured tensile strength was $F_a$ = 6.1 kN, considering all tested samples, with a coefficient of variation of 30%. From performed shear tests [6], an initial shear strength $f_{v,0}$ of 0.15 MPa was derived, with a friction coefficient μ of 0.78. These values exhibited a variation in the results of 10%. By considering the applied weight W on the connection (0.5 kN), it is possible to calculate the extraction force $F_e$ for a single brick's area $A_b$:

$$F_e = f_v A_b = f_{v,0} A_b + \mu W = \frac{[0.15 \cdot (210 \cdot 100 \cdot 2) + 0.78 \cdot 500]}{1000} = 7.1 \text{ kN}$$

In the calculation, the brick's surface is considered twice because the extraction takes place from the upper and lower brick.
It can be easily noticed that, depending on the variation of the results, it can happen that the brick's extraction occurs before the pull-out failure of the anchors, or vice versa:

- Upper bound anchor's strength: $F_a = 1.3 \cdot 6.1 = 7.93 \text{ kN} > F_e$
- Lower bound anchor's strength: $F_a = 0.7 \cdot 6.1 = 4.27 \text{ kN} < F_e$

This well explains why in the tested samples both failure modes were observed. It should be considered that the brick's extraction failure mode is much more likely to occur at the roof level (represented by the tested sample), because a very low weight is loading the masonry. At the other floor levels, the weight on each brick in which the anchors are fastened is preventing more its extraction.
This possible mixed failure mode has therefore to be taken into account when assessing the strength of this joint at roof level. Especially, it should be noticed that fastening the angle bracket with two anchors does not mean that the pull-out strength of the connection can be doubled, because of this potential mixed failure mechanism.

### 3.4.5 Configuration D

For connection type D, the same conclusions can be drawn as those discussed for configuration C. What is to be additionally considered, in this case, is the very important role played by the steel brackets. While the screws can again be calculated by means of Johansen's model, for the steel brackets the response has to be carefully evaluated, because of the three-dimensional distribution of forces: the calculation of the system composed of the steel angle and the screws can be performed by adopting the model shown in Figure 70. The horizontal load $F_h$ has to be transferred by this system to the bottom joist: $F_h$ is applied on the centre of mass of the existing joist, and therefore has an eccentricity *a* or *b* with respect to the centre of mass of each angle bracket, depending on the considered plane.
For the calculation, it can be assumed that the moment $M_v$ on the vertical plane is taken by the screws to be placed in that side of the angle bracket, together with the shear force; the moment $M_h$ on the horizontal plane follows the same principle. Since each screw is characterized by a certain stiffness, in practice rotations on both sides of the angle brackets can take place, and the screws could work also in tension because of this phenomenon, but this enables yielding and bending of both screws and angle brackets.
As it happened for configuration B, dynamic loading induced more play in the connection, which appeared to be less stiff. It is again suggested to combine the stiffness under dynamic behaviour with the safest estimation of strength obtained through both test types (for pulling the strength was lower under dynamic loading). This leads to the following modified constitutive law:

- Initial stiffness $K_0$: 1.74 kN/mm
- Peak force (+) $F_{max}$: 4.46 kN
- Peak force (-) $F_{max}$: 6.97 kN

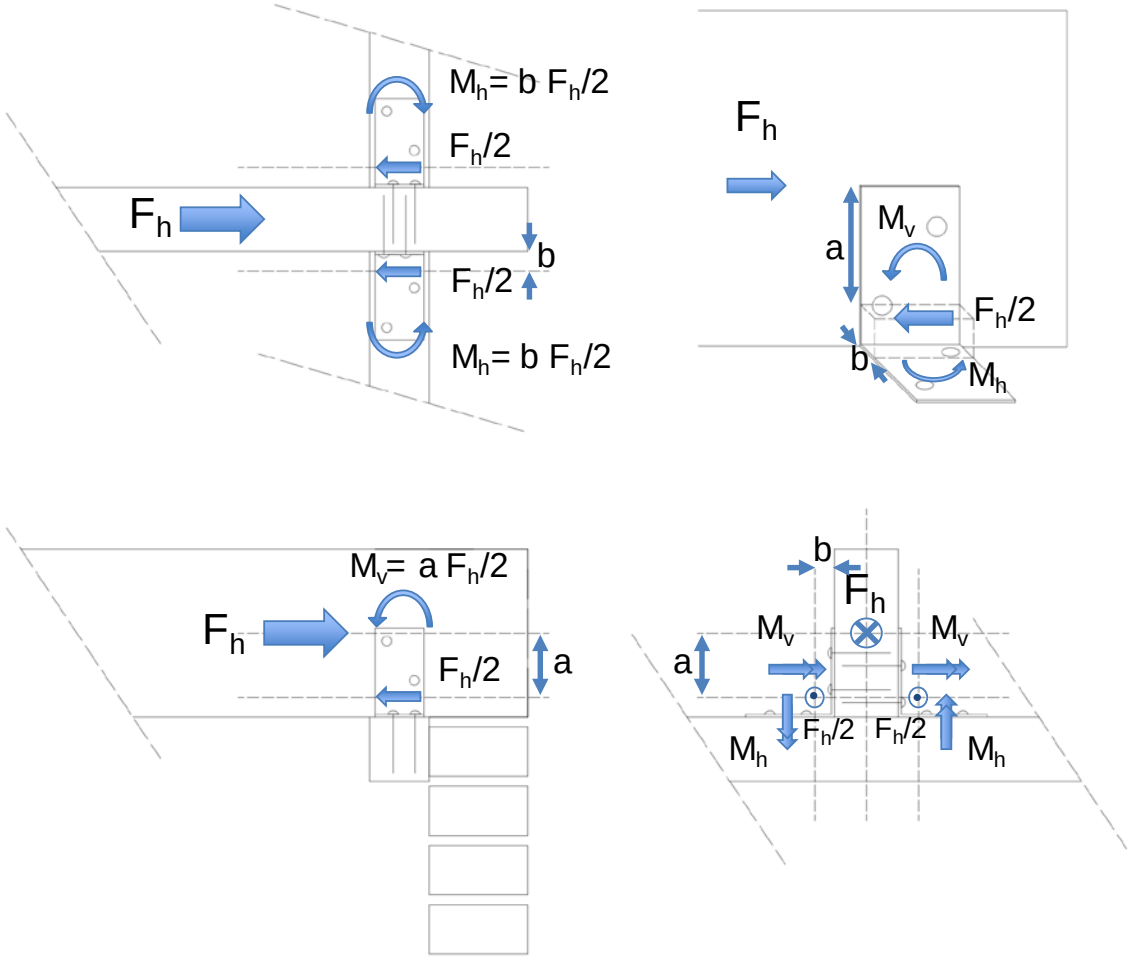


Figure 70 – Calculation model for the evaluation of the distribution of forces acting on the angle brackets and screws. Top left: top view; top right: 3D representation; bottom left: side view; bottom right: front view

### 3.4.6 Configuration E

For connection type E, the test results showed that the failure was brittle and related to the detachment of the outer layer of the wall around the glued pocket. Given the fact that the adopted hook anchor was a standard one and that approximately the same dimensions of the glued pocket could be realized in practice, it is recommended to consider the obtained pulling strength as a reliable estimation of the resistance of this joint. For this configuration, as shown in Figure 6, the glued pocket had dimensions of 25x40 mm and the same length as the hook anchor. It is therefore possible to calculate an equivalent shear stress $\tau_g$ corresponding to the detachment of this joint due to the failure of masonry around the glued interface:

$$\tau_g = \frac{F_{max,pulling}}{A_{glue\ pocket}} = \frac{4.42}{(25+40+40)\cdot 240} = 0.17\ \text{MPa}$$

This equivalent shear stress can then be used to calculate the detachment force also for different pocket dimensions. After this step, by knowing the force detaching the glued anchor, it is possible to design the nails of the hook anchor in such a way that they can provide energy dissipation. This is because the 4x55 mm nails used in the tested samples were also standard fasteners for the adopted hook anchor: however, by using more slender fasteners, a beneficial dissipative behaviour could be achieved, taking into account that the upper limit of the pulling strength is given by the detaching force. For the opposite direction, i.e. in pushing, the anchor is still able to transfer the horizontal load by contact, even after detaching, and this response can also induce bending and yielding when using more slender nails to fasten the hook anchor to

the joist. Like in the previous cases, the calculation for the nails is to be performed according Johansen's model.

### 3.4.7 Configuration F

For configuration F, the screws did not show failure in timber, but when calculating them a sufficient penetration length has to be ensured, according to the formulation for combined withdrawal and shear resistance in EC5. In the masonry, a mixed failure mechanism occurred, involving both brick extraction and flexural failure localized in the mortar bed joint. Brick extraction can again be referred to the area of a single brick, given the small distance between the screws, while the flexural failure is related to bond strength. From companion tests, this was measured as $f_b$ = 0.1 MPa [6]. By considering that the failure involves the whole wall width, the force causing the flexural failure is quantifiable as follows:

$$F_f = f_b A_{wall} = 0.1 \cdot 980 \cdot 100/1000 = 9.8 \text{ kN}$$

This value is very close to the range of observed values of connection strength [1], and considering the large dispersion affecting bond wrench test results, also for this case a combination of both flexural and extraction failure can occur. It should be noticed that the strength of this joint could me much higher at the other floors level, because of the larger weight loading the connection.
This failure type has in general to be considered and computed when the connection is particularly stiff and effective in transferring the shear load. As an example, configuration C, D and E in pushing are loading much more the wall compared to pulling direction, and therefore crack opening and flexural failures are more likely to occur. Of course, for a good estimation of this strength, the weight of masonry on top of the connection can be taken into account, whereas the parameter $A_{wall}$ is in practice given by the thickness of the wall multiplied by the heart-to-heart distance between the joists.
As a last consideration, it was observed that the glued layer did not fail, but caused cracks in the bricks or failures in the masonry, therefore it is not a governing or dominant behaviour. For calculation purposes, the screw can be considered as rigidly moving together with the brick(s) in which it is fastened.
Since in dynamic tests a higher play of the connection was observed, but also a higher strength in comparison to quasi-static tests, it is suggested to modify the constitutive law by using the values of strength from quasi-static tests and the stiffness from dynamic ones, with the following modified constitutive law:

- Initial stiffness $K_0$: 5.35 kN/mm
- Peak force (+) $F_{max}$: 8.52 kN
- Peak force (-) $F_{max}$: 6.25 kN

### 3.4.8 Configuration G

For configuration G, all fasteners for timber can be calculated according to Johansen's model. Again, it is important to notice that mixed failure mechanisms can occur, because of the mechanical anchors' pull-out failure or of the brick's extraction. This case (at least at roof level) is slightly worse if compared to configurations C and D, because there is no contribution of the weight of the joists, since the timber blocks are placed laterally to it. This means that only $f_{v,0}$ contributes to the strength, and that the extraction is in reality a shear failure of only the bed joint at the bottom of the brick in which the anchor is fastened, because only one row of bricks is above the one with the anchors (Figure 71). However, the fact that in total four anchors were placed at large distance, made possible to involve also three brick's surfaces, one and a half per side (the anchors closer to the joist were fastened to only half a brick). Therefore:

$$F_e = f_{v,0} 3 A_b = \frac{[0.15 \cdot (210 \cdot 100 \cdot 2) \cdot 3]}{1000} = 9.4 \text{ kN}$$

This value, combined with the flexural failure, explains again the range of results obtained during the experimental campaign. This range is close to these calculated values, and within their variation.

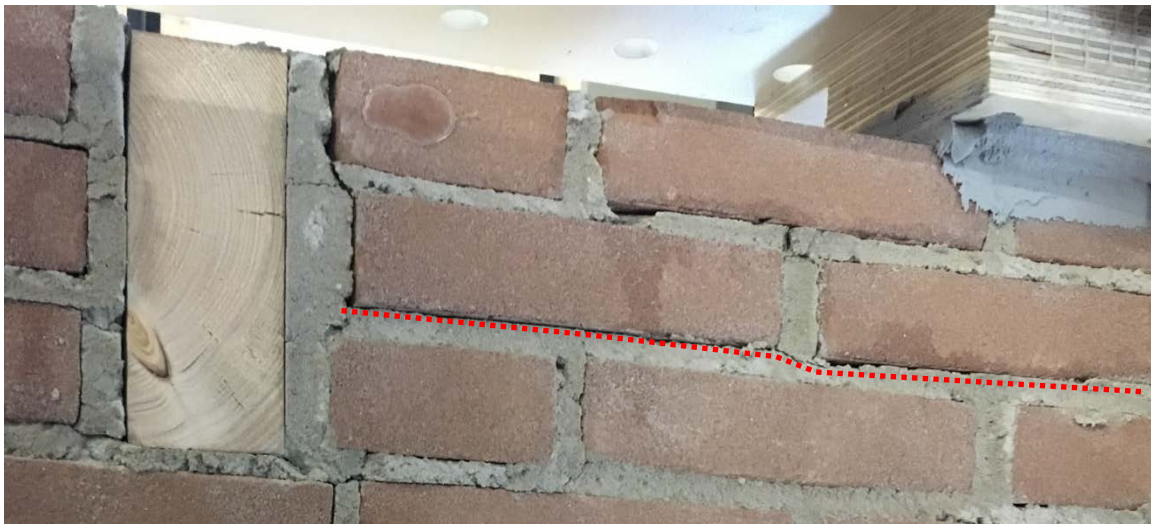

Figure 71 – Shear failure of the bricks' row in which anchors are fastened.

## 3.5 Damping properties of the connections

Timber-masonry connections can have beneficial properties in the global seismic response of a building, when it is possible to ensure an amount of energy dissipation in these joints without causing failure on them.
It should be noticed that high values of damping are not always associated to a proper behaviour of the connection under seismic load, because they could correspond to too large values of displacement or to values of force which are not sufficient to meet the demand.
The calculation of the equivalent damping ratio $\xi$ was conducted for quasi-static and dynamic tests by adopting the following equation [7]:

$$\xi = \frac{E_d}{4\pi E_e}$$

Where $E_d$ is the dissipated energy (area enclosed by the load cycle) and $E_e$ is the elastic energy (area given by the triangle whose sides are the peak force of the load cycle and the corresponding displacement).
This calculation was performed at a level of load which was approximately half of the peak for each connection, except for configuration A (for which the peak is constant), where this was done at half of the applied displacement. The results of this analysis are reported in Table 9 for both tests.
As can be noticed, configuration A showed the highest value because of its displacement capacity, but the limited load is not sufficient to prevent the walls from out-of-plane collapses. The other connections show values that were similar to each other: especially configurations C, D and G, thus the most ductile ones, showed remarkable damping values, if it is considered how they improved the stiffness and strength of the as-built configurations. Connection types E and F showed slightly lower values because they activated more brittle failure mechanisms
As can be noticed, the obtained values are quite similar between quasi-static and dynamic tests: therefore, the equivalent damping calculated from quasi-static tests can be regarded as a safe estimation of the actual one provided by the connection under dynamic loading. Only for configuration C the value obtained from dynamic tests is lower, but the variation in the results is also reduced compared to quasi-static tests. Furthermore, this is coherent to what was observed for this joint type when loaded dynamically, because it exhibited slightly narrower cycles with respect to quasi-static loading. Interestingly, all the connections that displayed an increased play under dynamic loading (configurations B, D, E and F), shown also higher damping values compared to quasi-static tests. Finally, configuration G exhibited the same damping value for both test types, confirming its reliability also from the dissipative point of view.
Therefore, the performed dynamic tests well show the influence of damping and confirm the results calculated from quasi-static tests.

Table 9 – Values of equivalent damping ratio $\xi$ calculated for each configuration under quasi-static (at half of the peak force) or dynamic loading (at 5 mm amplitude, corresponding in most cases to half of the peak force).

| Configuration | Equivalent damping ratio $\xi$ from quasi-static tests | Equivalent damping ratio $\xi$ from dynamic tests |
|---|---|---|
| A | 0.59 ± 0.03 | 0.61 ± 0.03 |
| B | 0.23 ± 0.03 | 0.37 ± 0.07 |
| C | 0.20 ± 0.08 | 0.15 ± 0.02 |
| D | 0.23 ± 0.05 | 0.24 ± 0.04 |
| E | 0.08 ± 0.02 | 0.15 ± 0.02 |
| F | 0.14 ± 0.02 | 0.15 ± 0.02 |
| G | 0.18 ± 0.03 | 0.18 ± 0.02 |

As a last consideration, these damping values can be inserted in Equation G.12 from NPR 9998 [9], where the single connection can be regarded as a subsystem to calculate the total $\xi$ of the whole building. It should be noticed that equation G.12 accounts not only for the damping of a certain structural element, but also for its strength: the combination of these two parameters influences then the global behaviour of the building, that can therefore be controlled from the dissipative point of view by means of this relation. In other words, depending on the cases, a certain connection type can be chosen in order to obtain the highest influence, even for such a small structural element, in terms of energy dissipation: this influence can be checked by means of the aforementioned equation.

# 4 Conclusions

In this document the interpretation of both testing phases for timber-masonry connections was presented. An analysis of the test results was conducted, together with the formulation of simplified models for the description of the behaviour of the connections, and the calculation and validation of their damping properties. The main failure modes for each configuration were highlighted, and constitutive laws followed by calculation methods were determined from the experimental data. Specific attention was placed in the characterization of the dynamic behaviour of the joints, especially with regard to their dissipative properties, which appeared to be quite significant for most of the tested connections. The formulated simplified rules and the derived relevant seismic properties of the joints can provide useful input for (nonlinear) numerical modelling, assessment of existing connections and design of strengthening methods for those that are not able to withstand seismic loads.

The main outcomes of this document are summarized for each configuration in Table 10. Figures 72 and 73 show an overview of all the constitutive laws of the joints for quasi-static and dynamic tests, respectively. Figures 74, finally, show an overview of the constitutive laws, modified taking into account the safest parameters (lower strength and/or stiffness), again for all configurations.

As a final remark, it is important to underline the precious contribution to this test campaign of dynamic tests. In general, they were useful to check the representativeness of quasi-static tests, but they provided quite some more information about damping properties, damage and behaviour of the connections under real seismic loads. Quasi-static tests can be regarded as a safe estimation of the actual behaviour of the connections, especially because influence of impact effects or sudden movements is not present. Moreover, the damage induced on the wall-connection system is usually larger, because of the repeated cycles. Instead, during dynamic tests less cycles are applied due to the very short signal, typical of Groningen.

The only attention should be paid to the possibility, especially for the stiffer connections, of a higher play (meaning a slightly decrease of stiffness) when they are subjected to dynamic loading, because this effect cannot be captured from quasi-static tests. Results showed, however, that this effect can even be reversed when the connection is strengthened with a system that distributes the load in a wide area, and not limitedly to the surface around the joist: this is exactly what was observed for configuration G, consisting of timber blocks placed on both sides of the joists. In that case, both strength and stiffness were larger under dynamic loading and no other connections displayed such an improved behaviour compared to quasi-static tests.

In order to safely estimate the behaviour of these configurations, it is advised to adopt the constitutive laws as reported in section 3.4 and Figure 74. The variety in strength, stiffness and dissipative properties of the joints appears to be beneficial for the application of the retrofitting techniques in contexts subjected to very different seismic demands.

Table 10 – Summary of the main outcomes from the characterization of tested connections

| Joint type | Failure mechanisms | Remarks from quasi-static tests | Remarks from dynamic tests | Recommendations for calculation | Ductile behaviour |
|---|---|---|---|---|---|
| A  | Friction on the joist-mortar interface. | Frictional response | Higher strength values due to sudden load | Use peak and post-peak friction coefficient | Yes, but with almost no transfer of load |
| B 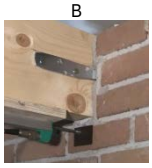 | • Friction on the joist-mortar interface;<br>• Yielding of nails;<br>• Cracking of masonry. | Whole wall activated in pulling after frictional behaviour | Higher play and lower stiffness | Use strength given by quasi-static tests, but stiffness from dynamic ones, because it is lower | Yes, but with almost no transfer of load in pulling |
| C 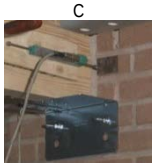 | • Yielding of screws;<br>• Cracking of masonry or bricks' extraction;<br>• Bending and yielding of the steel angle;<br>• Splitting in timber;<br>• Pull-out failure of the mechanical anchors. | Whole wall activated in both direction with effective transfer of load | Same stiffness, higher pushing strength due to impact effect | Check the possibility of mixed failures between brick extraction and pull-out failure of anchors | Yes |
| D  | • Yielding or pull-out failure of screws;<br>• Cracking of masonry or bricks' extraction;<br>• Bending and yielding of the steel brackets;<br>• Splitting in timber;<br>• Pull-out failure of the mechanical anchors. | Whole wall activated in both direction with effective transfer of load; yielding of screws and angle brackets | Higher play, lower stiffness; lower pulling strength and higher pushing strength | Use stiffness and pulling strength from dynamic tests, pushing strength from quasi-static ones | Yes |
| E  | • Yielding of nails;<br>• Cracking of masonry;<br>• Splitting in timber;<br>• Detachment of glue pocket with extraction of the hook anchor. | Whole wall activated in both direction with effective transfer of load until detachment of glued interface | Slightly higher pushing strength | To enhance ductile behaviour, nails' strength should be lower than the anchors' detachment one | No |
| F  | • Yielding or pull-out failure of screws;<br>• Cracking of masonry or bricks' extraction;<br>• Splitting in timber. | Whole wall activated in both direction with effective transfer of load and with very stiff behaviour | Higher play and lower stiffness, higher strength | Check the possibility of brick extraction or flexural failure for masonry | Limited |
| G  | • Yielding or pull-out failure of screws and nails;<br>• Cracking of masonry or bricks' extraction;<br>• Splitting in timber. | Whole wall activated in both direction with effective transfer of load and with very ductile behaviour | Higher strength and stiffness | Check the possibility of bricks' extraction or masonry cracking to correctly design nails | Yes |

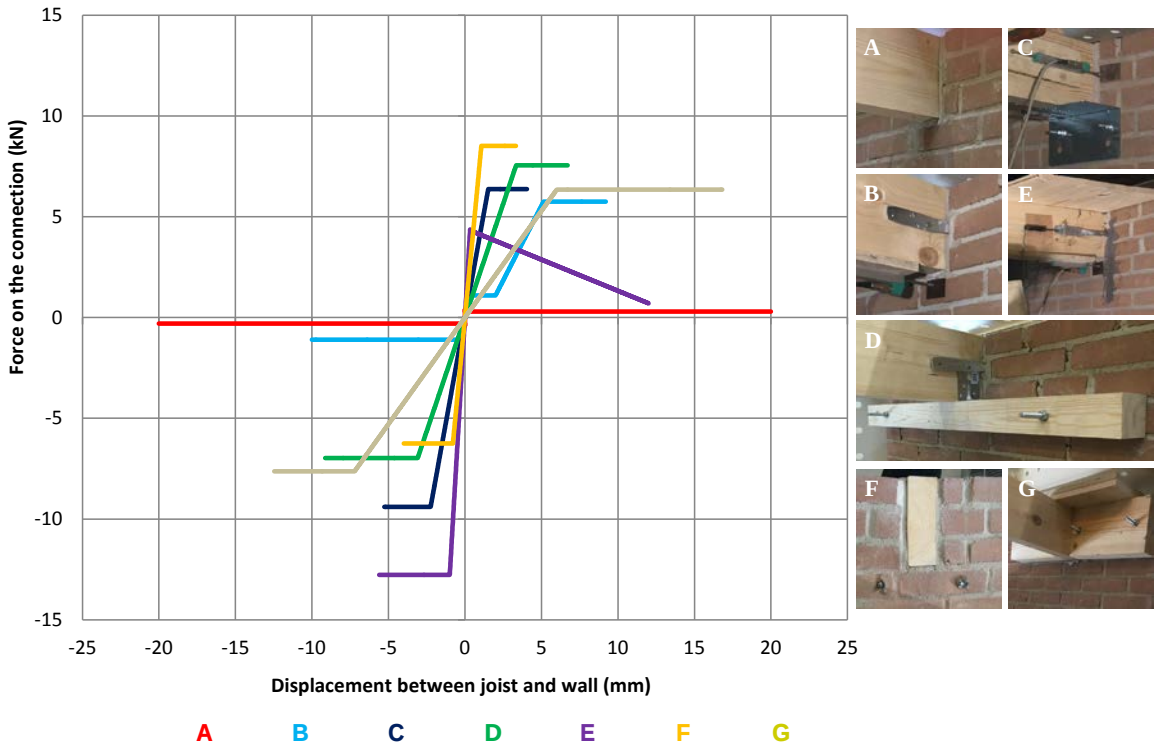


Figure 72 – Overview of the derived constitutive law referred to quasi-static tests

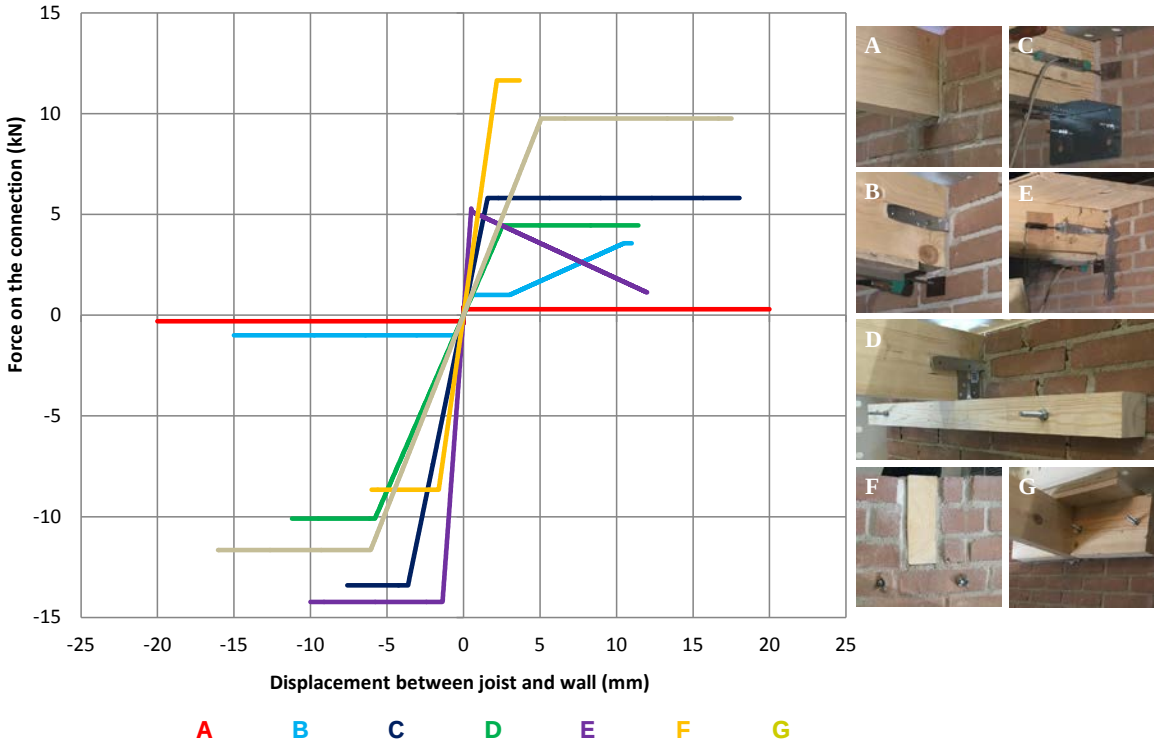


Figure 73 – Overview of the derived constitutive law referred to dynamic tests

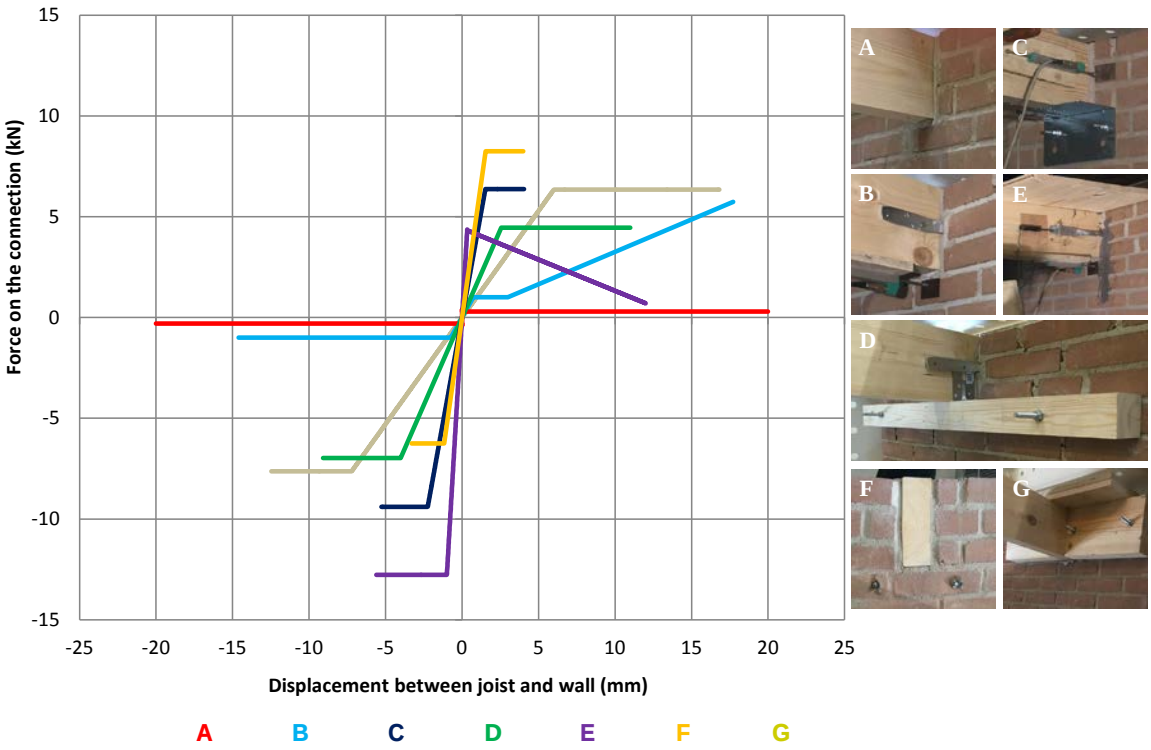


Figure 74 – Overview of the derived constitutive law with the safest parameters (lowest strength/stiffness)

# 5 References

[1] Mirra, M., Ravenshorst G. J. P. (2019). Monotonic, cyclic and dynamic behaviour of timber-masonry connections. Delft University of Technology. Report number CS2B04WP2-3.3, version 3, 3 December 2019.

[2] Messali, F., Ravenshorst, G.J.P. (2019). Database of connections: characteristics and properties. Delft University of Technology. Report number CM1B05-WP1-2.3, Final version, 03/12/2019.

[3] Arup Project Title: Groningen 2013 - Implementation Study, Document REP/229746/IS001, Issue Rev A, 29th November 2013

[4] EN 1995 (Eurocode 5): Design of timber structures. CEN, 1995.

[5] Licciardello, L., Mirra, M., Ravenshorst, G. J. P. (2019). Testing pull-out and shear capacity of Fischer mechanical anchors in clay brick masonry. Delft University of Technology.

[6] Licciardello, L., Esposito, R. (2019). Material tests for the characterisation of replicated solid clay brick masonry. TU Delft testing campaign 2019. Delft University of Technology. Report number CM1B04-WPC-2.3, 7 October 2019.

[7] Clough, R.W., Penzien, J., (1995). Dynamics of structures. Computer & Structures, Inc.

[8] EN 1998 (Eurocode 8): Design of structures for earthquake resistance. CEN, 1998.

[9] Nederlands Normalisatie-Instituut, NPR 9998 (2018).